TRACE MEASUREMENTS OF TELLURIUM, TIN AND OTHER METALS BY ATOMIC AND LASER SPECTROSCOPY TECHNIQUES

By

Sandeep Reddy Kunati

Submitted in Partial fulfillment of the Requirements

for the degree of

Masters of Science

in the

Chemistry

Program

YOUNGSTOWN STATE UNIVERSITY

AUGUST 2008

TRACE MEASUREMENTS OF TELLURIUM, TIN AND OTHER METALS BY ATOMIC AND LASER SPECTROSCOPY TECHNIQUES

Sandeep Reddy Kunati

I hereby release this thesis to the public. I understand that this thesis will be made available from the OhioLINK ETD Center and the Maag Library Circulation Desk for public access. I also authorize the University or other individuals to make copies of this thesis as needed for scholarly research.

Signature:

Sandeep Reddy Kunati, Student Date

Approvals:

Dr. Josef B. Simeonsson, Thesis Advisor Date

Dr. Larry S. Curtin, Committee Member Date

Dr. Roland Reisen, Committee Member Date

Peter J. Kasvinsky, Dean of School of Graduate Studies & Research Date

ABSTRACT

Sample introduction by using hydride generation (HG) technique enhances the sensitivity of certain hydride forming elements. In this study, methods have been investigated for the quantitative detection of Tellurium (Te), Tin (Sn), and other elements using HG coupled to Laser Induced Fluorescence (LIF), Laser Induced Breakdown Spectroscopy (LIBS), and Inductively Coupled Plasma Atomic Emission Spectroscopy (ICP-AES) detection techniques. In these studies, samples were subjected to HG and the resulting hydrides were carried to the flame atomizer in LIF, inductively coupled plasma in ICP-AES, and laser induced plasma in LIBS. The analytical figures of merit of these studies were evaluated to show the relative performance of each technique. The limits of detections (LOD) of Te and Sn were found to be 0.008 ppb and 0.07 ppb using HG-LIF, 1 ppm and 1 ppm using HG-LIBS and 2 ppm and 1 ppm using ICP-AES techniques. The results demonstrate that the combination of HG with LIF technique provides greater sensitivity as compared to the LIBS and ICP-AES techniques.

ACKNOWLEDGEMENTS

I would like to thank my research advisor, Dr. Josef B Simeonsson for his continuous advice, guidance, patience, help and encouragement throughout this project. I thank my committee members Dr. Larry Curtin and Dr. Roland Reisen for their time and patience. I would like to thank Dr. Muhsin Ezer for his help during the ICP-AES project. I would like to thank Dr. Roland Reisen and Ray Hoff for their help during the rectification of instrument problems. I would like to thank Ramnath, Ramana and Suman for their help and support during my masters program. I would like to thank Dr. Timothy Wagner and Dr. Daryl Mincey for their advisement and support during my graduate studies. Last but not least, I would like to thank my family for their support, encouragement, and blessings.

TABLE OF CONTENTS

TITLE PAGE ……...i

SIGNATURE PAGE …….……ii

ABSTRACT …….…....iii

ACKNOWLEDGEMENTS……...…….iv

TABLE OF CONTENTS …….....v-vii

LIST OF FIGURES …….……viii-x

LIST OF TABLES……xi-xii

LIST OF SYMBOLS AND ABBREVIATIONS……..……xiii-xv

CHAPTER I: INTRODUCTION……..…….1-10

1.1 Laser Induced Fluorescence……...……..1-2

1.2 Inductively Coupled Plasma Atomic Emission Spectroscopy……2-3

1.3 Laser Induced Breakdown Spectroscopy……3-5

1.4 Tellurium……..5-6

1.5 Tin……....6

1.6 Bismuth……..……..…7

1.7 Germanium……..…….……...7

1.8 Nickel….……..….8

1.9 Hydride Generation…….....8-9

1.10 Limit of Detection…….……10

CHAPTER II: GOAL OF THE PROJECT …….....11

CHAPTER III: INSTRUMENTATION……..12-31

3.1 Principle…….12-13

3.1.1 Laser Induced Fluorescence..……..……..……12

3.1.2 ICP-AES and LIBS……..……...…….....13

3.2. Laser Induced Fluorescence ……..…….....14-22

3.2.1 Nd:YAG laser……..……15-17
3.2.2 Tunable dye laser…….……...…..17-18
3.2.3 Frequency doubling crystal…….……...19
3.2.4 Optical systems…….……19
3.2.5 Detection system…….……..20-22
3.2.6 Oscilloscope……..…….....22
3.3 Inductively Coupled Plasma Atomic Emission Spectroscopy…….23-28
3.3.1 Sample introduction…….……24-25
3.3.2 Spray chamber…..……..25
3.3.3 Inductively Coupled Plasma…..……..…..……25
3.3.4 ICP torch…..…….26-27
3.3.5 Atomization of sample in ICP……..……27-28
3.3.6 Detectors……..……..…28
3.4 Laser Induced Breakdown Spectroscopy…….....29-31
3.4.1 LIBS Plasma…….……....31
CHAPTER IV: EXPERIMENTAL METHODS..……32-40
4.1 Chemicals and materials……...……..32
4.2 Experimental setup for LIF…..……...……33-35
4.3 Experimental setup for ICP-AES…..…….……..…36
4.4 Experimental setup for LIBS..……..…….……..…...37-39
CHAPTER V: RESULTS AND DISCUSSION..……..…….....41-85
5.1 Laser Induced Fluorescence…….41-48
5.1.1 Optimal conditions used for HG-LIF…….....41-45
5.1.2 Calibration and analytical figures of merit…….……..45-48
5.2 ICP-AES…….…….....49-67
5.2.1 Bismuth…….....49-51
5.2.1.1 Calibration curve……..49-51
5.2.2 Tin……..……...52-54
5.2.2.1 Calibration curve……..52-54
5.2.3 Tellurium…..…….....55-57
5.2.3.1 Calibration curve……..55-57

5.2.4 Response of plasma torch to different acid and hydride conc…...57
5.2.5 Nickel……....58-59
5.2.5.1 Calibration curve……..58-59
5.2.6 Zinc……..……...…….....60-61
5.2.6.1 Calibration curve……..…….……...60-61
5.2.7 Germanium…..…….……..…….....62-63
5.2.7.1 Calibration curve……..62-63
5.2.8 Cobalt…….…..……64-65
5.2.8.1 Calibration curve……..…….…….…..64-65
5.2.9 Detection of elements in a std. solution using ICP-AES…….....66
5.2.10 Comparison of ICP-AES and HG-ICP-AES…….67
5.3 Laser Induced Breakdown Spectroscopy….……....68-85
5.3.1 Studies using 355 nm Laser…….....68-72
5.3.1.1 Tellurium……..68-72
5.3.1.1.1 Study of different parameters…….68-70
5.3.1.1.2 Wavelength selection…..…….71
5.3.1.1.3 Analytical figures of merit……..……72
5.3.2 Studies using 532 nm Laser…….....73-85
5.3.2.1 Arsenic……..……...….73-76
5.3.2.1.1 Study of different parameters…….73-74
5.3.2.1.2 Wavelength selection…..…….75
5.3.2.1.3 Analytical figures of merit…….…….....76
5.3.2.2 Tin…..……..……...….77-80
5.3.2.2.1 Study of different parameters…….77-78
5.3.2.2.2 Wavelength selection…..…….79
5.3.2.2.3 Analytical figures of merit…….....80
5.3.2.3 Enhancement effect of ethanol……..…….....82
5.3.2.4 Detection of different metals in mixture……83
5.3.2.5 Hydrogen emission spectra……...84-85
CHAPTER VI: CONCLUSIONS AND FUTURE WORK.…….86-87
CHAPTER VII: REFERENCES……..…….....88-94

LIST OF FIGURES

Figure 1: Laboratory used hydride generator ……..…….……..9

Figure 2: Schematic diagram of Atomic Fluorescence Spectroscopy ……..12

Figure 3: Schematic diagram of Atomic Emission Spectroscopy ……13

Figure 4: Schematic diagram of Te-HG-LIF ……14

Figure 5: Schematic diagram of Nd:YAG laser……15

Figure 6: Laboratory used Nd:YAG laser……..…….……..16

Figure 7: Laboratory used Tunable dye laser…….…….…….....18

Figure 8: Molecular structure of stilbene ……..…….……..18

Figure 9: Configuration of frequency doubling crystal…….…….……...19

Figure 10: Schematic diagram of Czerny-Turner grating monochromator……..….....20

Figure 11: Schematic diagram of Photo-Multiplier Tube (PMT)……..22

Figure 12: Laboratory used Oscilloscope…….....22

Figure 13: Schematic Diagram of HG-ICP-AES …….……22

Figure 14: Laboratory used ICP-AES……..……..……...24

Figure 15: Schematic diagram of pneumatic nebulizer and spray chamber…….…....25

Figure 16: Formation of ICP torch ……..……..……27

Figure 17: Sample ionization in the plasma ……..……...28

Figure 18: Schematic diagram of LIBS……29

Figure 19: Laboratory used Boxcar integrator…….…….....30

Figure 20: Laboratory produced LIBS plasma…….…….31

Figure 21a: Influence of hydrochloric acid conc. on fluorescence intensity…….42

Figure 21b: Influence of sodium tetrahydroborate conc. on fluorescence intensity…....42

Figure 21c: Influence of peristaltic pump flow rates on fluorescence intensity ……..43

Figure 21d: Influence of monochromator slit width on fluorescence intensity……44

Figure 22: Power dependence curve……..…45

Figure 23: Calibration curve for Te-HG-LIF ……..…….46

Figure 24: Calibration curve for Sn-HG-LIF…….……...46

Figure 25a: Calibration curve for Bi-ICP-AES…….…...……49

Figure 25b: Calibration curve for Bi-HG-ICP-AES ……..…..….50

Figure 26a: Calibration curve for Sn-ICP-AES ……...52

Figure 26b: Calibration curve for Sn-HG-ICP-AES……...…..53

Figure 27a: Calibration curve for Te-ICP-AES…….55

Figure 27b: Calibration curve for Te-HG-ICP-AES…….....56

Figure 28a: Calibration curve for Ni-ICP-AES……..…...58

Figure 29a: Calibration curve for Zn-ICP-AES …….…...60

Figure 30a: Calibration curve for Ge-ICP-AES……62

Figure 31: Calibration curve for Co-ICP-AES…….……...…….64

Figure 32a: Te emission spectra at different gate widths……..69

Figure 32b: Te emission spectra at different time delays…….…….....69

Figure 32c: Te emission spectra at different detector slit widths ……..…70

Figure 32d: Te emission spectra at 214.28 nm…….....71

Figure 32e: Calibration curve of tellurium at 214.28 nm……72

Figure 33a: As emission spectra at different gate widths ……73

Figure 33b: As emission spectra at different detector slit widths…..……74

Figure 33c: As emission spectra at 197.3 nm wavelength.……...75

Figure 33d: Calibration curve for arsenic at 197.3nm……..…76

Figure 34a: Sn emission spectra at different delays ……77

Figure 34b: Sn emission spectra at different gate widths ……78

Figure 34c: Sn emission spectra at 270.65 nm……..…....79

Figure 34d: Calibration curve for tin at 270.65 nm ……..……80

Figure 35: Enhancement effect of ethanol on arsenic and tin sensitivity……..……....82

Figure 36: Detection of different metals in a mixture ……..…….....83

Figure 37a: Hydrogen emission spectra near 656 nm…….……..……....84

Figure 37b: Hydrogen emission spectra near 486 nm…….……..……....85

Figure 37c: Hydrogen emission spectra near 434 nm…….……..……....85

LIST OF TABLES

Table 1: Wavelengths of Nd:YAG laser……..…….……16

Table 2: Energy of fundamental and harmonic wavelengths of Nd:YAG laser……17

Table 3: Specifications of the laboratory Nd:YAG laser….…….……17

Table 4: Specifications of laboratory Czerny-Turner monochromator……..……..21

Table 5: Experimental conditions used for LIF…….……..…..…34

Table 6: Experimental conditions used for tellurium and tin in LIF.……..….35

Table 7: Experimental conditions used for the ICP-AES measurements…….….36

Table 8: Experimental conditions used for LIBS…….……..…38

Table 9: Experimental conditions used for arsenic, tellurium and tin……..….39

Table 10: Transition probabilities of elements……..……40

Table 11: Peristaltic pump flow rates of acid, sodium borohydride and sample…....….43

Table 12: Optimal conditions for HG-LIF……44

Table 13: UV absorption rate of the ND filters at different wavelength.…..……47

Table 14: Analytical figures of merit for HG-LIF….……..…….……48

Table 15: Comparison of HG-LIF with previous techniques..…….….48

Table 16: LOD's of bismuth at different wavelengths …….……50

Table 17: Comparison of Bi-ICP-AES with other techniques.…….……51

Table 18: LOD's of tin at different wavelengths……..……53

Table 19: Comparison of Sn-HG-LIF with other techniques…….……..…….54

Table 20: Comparison of Te-ICP-AES with other techniques…….…….56

Table 21: Response of plasma torch to different acid and borohydride concentrations…57

Table 22: LOD's of Nickel at different wavelengths…..……..…….58

Table 23: Comparison of Ni-ICP-AES with other techniques…….…..…59

Table 24: LOD's of zinc at different wavelengths…….……..…….60

Table 25: Comparison of Zn-ICP-AES with other techniques…….…….61

Table 26: LOD's of germanium at different wavelengths…….…….……..……62

Table 27: Comparison of Ge-ICP-AES with other techniques……..……63

Table 28: LOD's of cobalt at different wavelengths.…….……..….64

Table 29: Comparison of Co-ICP-AES with other techniques……..…….……..…65

Table 30: Elements and their uncertainties found in standard solution…..……..…….66

Table 31: Comparison of LOD of ICP-AES and HG-ICP-AES……...…..……67

Table 32: Analytical figures of LIBS…….……..……81

Table 33: Comparison of HG-LIBS with other techniques..……..……..……81

LIST OF SYMBOLS AND ABBREVIATIONS

LASER…….…… Light Amplification by Stimulated Emission of Radiation

Nd:YAG……Neodymium-doped yttrium aluminum garnet

LIF…….……Laser Induced Fluorescence

LIBS……..……..Laser Induced Breakdown Spectroscopy

ICP-AES……Inductively Coupled Plasma Atomic Emission Spectroscopy

HG……..……Hydride generation

PMT……..……Photomultiplier tube

RF……..…..…….…Radiofrequency

Nd^{3+}……Neodymium ion

Te…….…..…….……...Tellurium

Sn……..……...Tin

As…….……Arsenic

Bi……..……...Bismuth

Ge……Germanium

Ni……..……..Nickel

Zn…….……...Zinc

Co…….……...Cobalt

Ar…….……Argon

H_2……...Hydrogen

He…….……..Helium

ppm…….…….Parts per million

ppb……..……..Parts per billion

ppt……..……..Parts per trillion

LOD…….……Limit of detection

LOQ……..……Limit of quantification

RSD……Relative standard deviation

HCl……Hydrochloric acid

$NaBH_4$……..…….……..…..……Sodium Borohydride

NaOH……..…….Sodium hydroxide

L.……Liter

mL……Milliliter

µg…….…….……..…….Microgram

Cm…….……..Centimeter

mm……..…..Millimeter

nm……Nanometer

µs……...……Microsecond

ns…….…...Nanosecond

µm……...Micrometer

M……..……Molar

m/v……..……...mass per volume

v/v……..volume per volume

V……..…….……..Volt

mV…….……..……Millivolt

eV……..……..…Electronvolt

kW……Kilowatt

mJ…….……..……Millijoule

mrad…….……Milliradian

Hz…….……Hertz

MHz……..…Megahertz

K……..……Kelvin

^{o}C……..…….Degree Celsius

min…….…….minute

% …….....percentage

a.u.……..……..…arbitrary units

CHAPTER I

INTRODUCTION

Elemental analysis methods are important for studying the effects of environmental pollution by metals and metalloids. Elemental speciation analysis methods are becoming more important because of the dependence of the toxicity, bioavailability, and mobility on the element's chemical form.[1] Several atomic spectroscopy techniques have been used previously for the detection of various elements in environmental and biological samples. In this project, Laser Induced Fluorescence (LIF), Inductively Coupled Plasma Atomic Emission Spectroscopy (ICP-AES) and Laser Induced Breakdown Spectroscopy (LIBS) techniques have been evaluated for the detection of several trace elements including Tellurium, Tin, Arsenic and other metals.

1.1. LASER INDUCED FLUORESCENCE (LIF)

Laser Induced Fluorescence is a type of Atomic Fluorescence in which atoms are excited by absorbing laser light and emit fluorescence as they return to a lower state. The major advantages of LIF compared to other techniques are high selectivity due to the use of different emission and excitation wavelengths and high sensitivity due to the high signal to noise ratio of the fluorescence signal. Laser Induced Fluorescence is a sensitive and selective analytical method for trace elemental analysis with detection limits down to ppt levels.[2] It can be used in the analysis of complex samples without loss of sensitivity.[3] The detection limits obtained with LIF are often comparable to ICP-MS. Advantages of LIF over ICP-MS can include a lower order of magnitude of absolute LOD, which is

important in the case of limited sample volume, and high selectivity that minimizes spectral interferences.[4]

1.2. INDUCTIVELY COUPLED PLASMA ATOMIC EMISSION SPECTROSCOPY (ICP-AES)

Inductively Coupled Plasma Atomic Emission Spectroscopy is a type of Atomic Emission Spectrometry, in which high energy plasma is used to thermally excite analyte atoms and the atoms emit energy in the form of photons which can be detected and quantified when they return to a lower state. Inductively Coupled Plasma Atomic Emission Spectroscopy (ICP-AES) is one of the most widely used analytical methods for the detection of trace metals in biological and environmental samples.[5]

This method has been used for the analysis of both liquid and solid samples. Attractive features of ICP-AES include low running costs, ease of use, elimination of chemical interferences, multi-element analysis, and reproducible and accurate results. Its multi-element capability allows measurements of 5-20 elements per sample. As many as 70 elements can be analyzed by this approach. The measurement range can extend from the parts per billion (ppb) to percentage levels because of the high linear dynamic range (10^5). The detection limits can be improved by purifying the samples, using chromatography techniques, and using different sample introduction techniques, including hydride generation sample introduction.

The ICP-AES method can suffer from matrix effects and spectral and ionization interferences. Spectral interferences can often be controlled by using a high resolution monochromator, and inter element correction. Ionization interferences can be reduced by

changing the sample conditions such as adding a buffer solution to the sample. Matrix effects in samples can also be controlled by using internal standards.[6,7]

1.3. LASER INDUCED BREAKDOWN SPECTROSCOPY (LIBS)

Laser Induced Breakdown Spectroscopy (LIBS) is an analytical atomic spectroscopic method that is also called Laser Induced Plasma Spectroscopy (LIPS) or Laser Spark Spectroscopy (LSS). Laser Induced Breakdown Spectroscopy is a type of Atomic Emission Spectrometry in which a high energy laser pulse is used to create hot plasma that can be used to atomize and excite analyte samples. The excited atoms or ions emit energy in the form of photons, which can be measured.

In LIBS, elemental analysis is based on photon emission from the sample due to a laser produced plasma, so it can be used for direct and in situ measurements of solids,[8] liquids,[9] and gaseous[10] samples including aerosols, gels, and slurries. It is used for direct quantitative analysis of solids like ceramics and semiconductors, which are hard to dissolve or digest.[11] It can be operated in standoff mode and requires only a small amount (nanograms to picograms) of sample. Direct analysis minimizes possible contamination that can occur during the sample preparation process. The LIBS approach is useful due to its simple operating procedure, in-situ measurement ability, lack of sample preparation, non-destruction or minimal destruction of the sample, multi-element capability, rapid analysis, high spatial resolution, and low detection time (normally less than a second). It has been used in elemental analysis of solutions, in-situ biological analyses, quality control of industrial processes, environmental monitoring,[12,13] on-line industrial monitoring, chemical imaging, hazardous and explosive environmental monitoring,[14]

identification of carious teeth,[15] identification of particle size and chemical composition in aerosols,[16] analysis of artifacts in archeology, identification of biological weapons in defense, identification of nuclear waste disposals in nuclear industry, and space exploration.

The disadvantages of LIBS include relatively low sensitivity, poor accuracy (about 10%), and precision (up to 5%), matrix effects, spectral interferences, particle size interferences in aerosols[17] and changes in the laser pulse energy with surrounding environmental conditions. The Limit of Detection (LOD) typically ranges from 0.1 ppm to 200 ppm, depending upon the sample type, type of laser used, and apparatus conditions. Matrix effects of samples can be reduced by using internal standards,[6,7] and spectral interferences can be reduced by using a high resolution monochromator, inter-element correction and dynamic background correction as in other atomic emission approaches.

Laser Induced Breakdown Spectroscopy can be used for detection of all elements depending upon the laser pulse energy and laser wavelengths. Almost all elements are excited by the high temperatures of the plasma (10,000 to 20,000 K). The LIBS approach has been used for analysis of chlorinated hydrocarbons in aqueous solutions,[18,19] alkali metals,[20] and alkaline earth metals[21] in aqueous solutions, Li, Na, Mg, Ca, Mn, and Al in aqueous solutions,[22] Rb, Li, and Cd in a liquid jet,[23] Na,[24] K,[25] and Ba[26] in aqueous solutions. It has also been used for analysis of As and Sn by hydride generation,[27] As, B, and P in gases,[28] and Be, Na, P, As, and Hg in air.[29] It has also been used for molecular analysis,[30] determinations of alloy compositions,[31] for corrosive and hazardous environments[32] in a stand-off mode and even for analyses on Mars (ExoMars).[33]

In this project, several elements including Tellurium (Te), Tin (Sn), Arsenic (As), Bismuth (Bi), Germanium (Ge), and Nickel (Ni) have been studied using the above mentioned methods. Their characteristics and importance for detection are summarized below.

1.4. TELLURIUM

Tellurium is a non-essential element that is found in trace amounts in the earth's crust. It has a wide range of applications in metal, glass, plastic, and pharmaceutical industries, and as a semi- conductor in electronics,[34] which are considered the major sources of tellurium contamination in the environment. In nature, tellurium can occur as tellurite [TeO_3^{2-}, Te (IV)] and tellurate [TeO_4^{2-}, Te (VI)] [35] with other metals like gold, silver, lead and bismuth. As compared to Te (IV), Te (VI) is more abundant but less stable in nature. In natural waters, tellurium is generally found at sub-ppt levels.[36] It is toxic to humans in a concentration of 0.01 ppm or less in air. For persons who are exposed, it can give a strong garlic-like odor due to the formation of dimethyl telluride and it accumulates in the heart, kidney, spleen, bone and lungs.[37] It is important to develop more sensitive and improved methods of analysis for tellurium in environmental and biological samples.[38]

Tellurium exists in different oxidation states including -2, +2, +4 and +6. Tellurite (IV) is considered to be 10 times more toxic than tellurate (VI).[39] Many approaches have been proposed for the speciation of tellurium including Atomic Absorption Spectroscopy (AAS),[40] Atomic Emission spectroscopy (AES),[41] Atomic Fluorescence Spectroscopy (AFS),[42] Graphite Furnace Atomic Absorption Spectroscopy (GFAAS),[43] Inductively

Coupled Plasma Atomic Emission Spectrometry (ICP-AES)[44] and Inductively Coupled Plasma Mass Spectrometry (ICP-MS)[45] in combination with Liquid Chromatography (LC-ICP-MS),[46] Ion Chromatography (IC)[47] or High Performance Liquid Chromatography techniques (HPLC).[48]

1.5. TIN

Tin and organo-tin compounds are used as plating materials for food storage, and as an additive and coating material in paints.[49] Tin can be found in large concentrations in water, soil and biological samples.[50] Tributyltin chloride (TBT) and its degradation products dibutyltin (DBT) and monobutyltin (MBT) often accumulate in marine organisms and are considered to be marine contaminants.[51] The biodegradation of these compounds takes several years.[52]

Metallic tin in a concentration more than 200 ppm is toxic to humans.[53] Due to its low solubility and low absorption rate, ingested tin has low toxicity.[54] It can be absorbed through food, air, and skin and may cause severe health defects in growth, reproduction and enzymatic systems. TBT may also cause infertility by altering hormonal balances. Previously used techniques for the speciation of tin include Atomic Fluorescence Spectroscopy (AFS),[55] Flame Atomic Absorption Spectrometry (FAAS),[56] Electrothermal Atomic Absorption Spectrometry (ETAAS),[57] Mass Spectrometry (MS),[58] Inductively Coupled Plasma Atomic Emission Spectrometry (ICP-AES),[59] and Inductively Coupled Plasma Mass Spectrometry (ICP-MS)[60] in combination with Liquid Chromatography (LC-ICP-MS),[61] or High Performance Liquid Chromatography techniques (HPLC).[5]

1.6. BISMUTH

Bismuth compounds are used as medications to treat several diseases.[62,63] They are also used as starting materials for rubber and synthetic fibers and as carriers for uranium isotopes. In nature, bismuth is found as bismuthinite (bismuth sulfide) and bismite (bismuth trioxide). Bismuth is not considered to be a major problem in the environment and is not considered to be toxic to humans, but ingestion of small amounts of bismuth medications may lead to neurotoxicity and motor dysfunction.[64] Due to its low concentration in the environment, it requires highly sensitive methods for detection. The previously used techniques for bismuth detection are AFS,[65] ICP-AES,[66] ICP-MS.[67] HG-AAS,[68] HG-ICP-AES[69] and HG-ICP-MS.[70]

1.7. GERMANIUM

Germanium is usually found in the earth's crust in the form of argyrodite (GeS_2 and Ag_2S) and germanite (GeS_2, FeS, Cus). Organo-Germanium compounds are used as antioxidants, and immunostimulators.[71] Germanium is used as a semiconductor in transistors, and integrated circuits in fiber optics, communication networks, wide angle lenses, and infrared night vision systems. Its heavy metal nature can cause some negative impact on the environment and germanium is considered to be an environmental pollutant. Due to its low concentration in environmental samples, it requires highly sensitive methods for detection. The previously used techniques for germanium analysis are ETAAS,[72] AFS,[73] ICP-MS,[74] HG-AAS,[75] HG-AFS,[76] HG ICP-AES[77] and HG-ICP-MS.[78]

1.8. NICKEL

Nickel is a trace element usually found in low concentrations in the environment. It is normally found in natural waters at a concentration of 1.5 ppb.[79] Nickel is mainly used in the form of alloys with iron, chromium and other metals in the production of stainless steel. The major source of nickel in the environment is from industrial sources and it accumulates in water and soil. Humans are exposed to nickel in low concentrations through air, water and food sources. These exposures may result in pneumonia and carcinoma. The maximum allowable quantity of nickel in natural waters is 20 ppb. Due to its usually low concentration in real samples, it requires highly sensitive methods for detection. The previously used techniques for Nickel analysis are AAS,[80] ETAAS,[81] AFFS,[82] ICP- AES,[83] FI-ICP-AES,[84] and ICP-MS.[85]

1.9. HYDRIDE GENERATION (HG)

Hydride generation (HG) is sample introduction method used to convert dissolved metal and metalloid ions into their gaseous metal hydrides.[86] Continuous flow hydride generation is considered to be one of the most useful sample introduction techniques for speciation analysis of hydride forming elements. The major advantage of HG is it greatly increases the sample efficiency and sensitivity resulting in lower detection limits. The main drawback of this technique is that it requires a particular oxidation state of the element before formation of the hydride.

The hydride generation system consists of a 4-channel peristaltic pump (Rainin, dynamax RP-1, CA, USA), a U-shaped gas-liquid separator and a Nafion tube dryer

(Figure 1). The peristaltic pump uses 1 mm, 1 mm and 2 mm diameter tubing with flow rates of 8 mL min^{-1}, 8 mL min^{-1} and 14 mL min^{-1} to pump HCl, $NaBH_4$ and sample solutions, respectively, in a continuous flow pattern. These three solutions are mixed in a chamber and flow through a reaction coil to a U-shaped gas-liquid separator, which separates the gas from the liquid and purges the volatile hydride towards the atomizer. A helium or argon gas stream (approximately 200 mL min^{-1}) is used to deliver the volatile hydride into the atomizer.

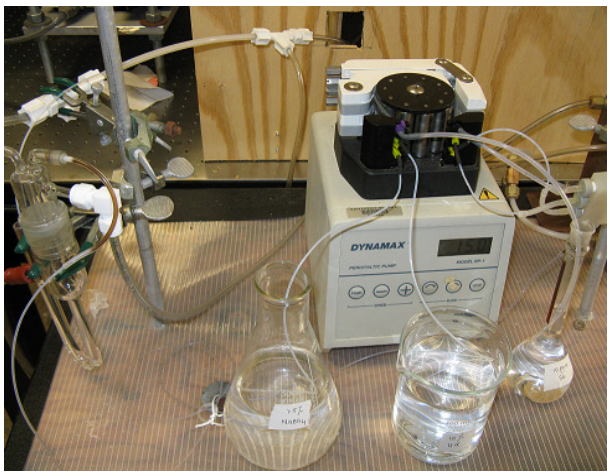

Figure 1 Laboratory used hydride generator

Atomic Fluorescence Spectroscopy in combination with hydride generation has shown high sensitivity for the determination of atomic species such as As,[87] Se,[40] Sb,[63] Te,[74] Bi,[88] and Ge.[89] The combination of HG with different atomic spectroscopic techniques has shown promising results for tellurium[90,91,92,93,94] and tin.[55,59,60,61,95,96] Most hydride forming elements are detected by using AFS in the region below 250 nm because of the low background emission and the simplicity of the spectra due to the separation of analyte from the matrix.[97]

1.10. LIMIT OF DETECTION (LOD)

The limit of detection (LOD) is the smallest amount of analyte in a sample that can be detected. According to IUPAC, the LOD is estimated from the mean of the blank, the standard deviation of the blank and a confidence factor.

$$X_L = X_{bi} + ks_{bi}$$

X_L = Limit of Detection (smallest signal that can be detected)

X_{bi} = mean of blank measurements

s_{bi} = standard deviation of the blank measurements

k = confidence level

By converting X_L into units of concentration C_L, the LOD can be expressed as

$$C_L = C_{bi} + ks_{bi}/m$$

Where m is the sensitivity or slope of the calibration curve and is the response as a function of analyte concentration. High sensitivity means a large response and a good detection limit.

In these studies, the limit of detection (LOD) is calculated using k=3 and the LOD is expressed as a concentration in ppb or ppm.

CHAPTER II

GOAL OF THE PROJECT

The main goal of the project is to investigate several methods and develop selective and sensitive techniques for the measurement of tellurium, tin, and other elements using Laser Induced Fluorescence (LIF), Inductively Coupled Plasma Atomic Emission Spectroscopy (ICP-AES) and Laser Induced Breakdown Spectroscopy (LIBS) approaches. Optimization of the methods is performed by investigating experimental parameters and evaluating analytical figures of merit including the Limit of Detection. The analytical utility of these approaches is further evaluated by comparing the results to other methods.

CHAPTER III

INSTRUMENTATION

3.1. PRINCIPLES

3.1.1. LASER INDUCED FLUORESCENCE (LIF)

Atomic Fluorescence Spectroscopy can be viewed as a method having the characteristics of both Atomic Absorption Spectroscopy (AAS) and Atomic Emission Spectroscopy (AES) methods. Laser Induced Fluorescence (LIF) is a type of Atomic Fluorescence Spectroscopy (AFS) approach where a laser is used as the light source.

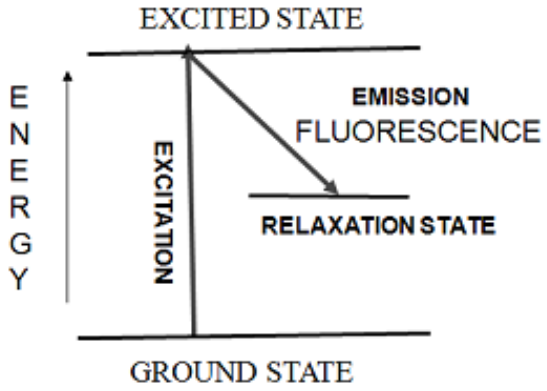

Figure 2 Schematic diagram of Atomic Fluorescence Spectroscopy

The principle involved in this technique is fluorescence emission, which is a two step process involving excitation and relaxation. Atomic excitation is caused by the absorption of photon energy from incident radiation. The excited state atom then relaxes by reemitting the energy in the form of fluorescence emissions. Atomic Fluorescence Spectroscopy is a useful method for quantitative measurements of elements because of its wavelength selectivity, its high signal to noise characteristics and low background noise.

3.1.2. ICP-AES AND LIBS

Inductively Coupled Plasma Atomic Emission Spectroscopy (ICP-AES) and Laser Induced Breakdown Spectroscopy (LIBS) are both emission spectroscopic techniques in which atoms are thermally excited and the energy emitted during relaxation is observed in the form of electromagnetic radiation (hν).

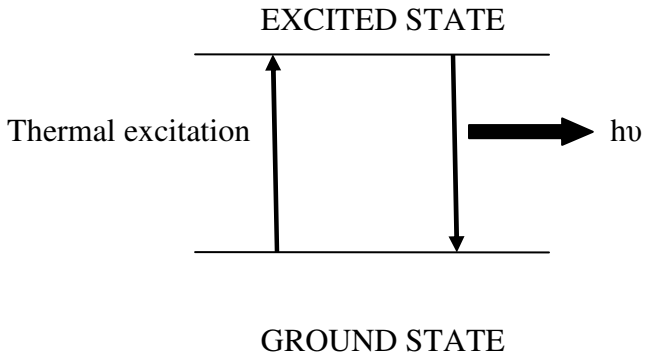

Figure 3 Schematic diagram of Atomic Emission Spectroscopy

In atomic emission spectroscopy, each element emits light at specific wavelengths. The emitted photons are measured and the quantity of this energy is proportional to the concentration of that element in the sample. By comparing the intensity of an unknown with a standard, the elemental concentration of an unknown can be determined.

3.2. LASER INDUCED FLUORESCENCE (LIF)

In Laser Induced Fluorescence, electrons in atoms absorb energy from a laser excitation source, become excited and emit fluorescent radiation. Laser Excitation provides selective excitation of the analyte which helps to avoid interferences.

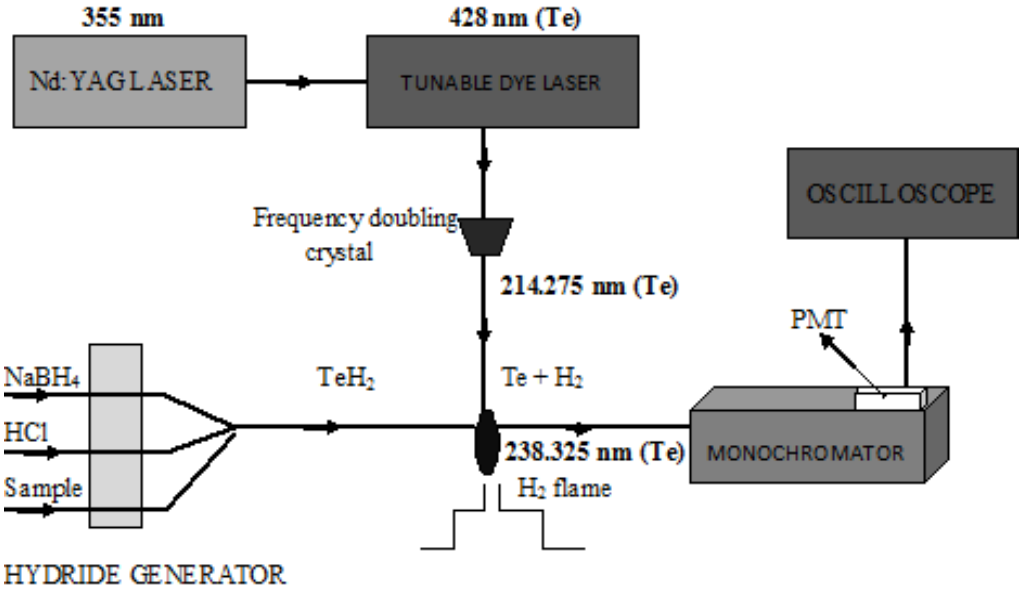

Figure 4 Schematic diagram of Te-HG-LIF

The LIF instrumentation in this project consists of

1. Nd:YAG laser (pulsed laser)
2. Tunable dye laser
3. Frequency doubling crystal
4. Optics for focusing and collecting light
5. Detection system consisting of a monochromator and a detector
6. Oscilloscope and computer to view and record the spectrum

3.2.1. Nd:YAG LASER

A Nd:YAG pulsed laser is used as a light source in LIF (Continuum, SureLite SLII-10).

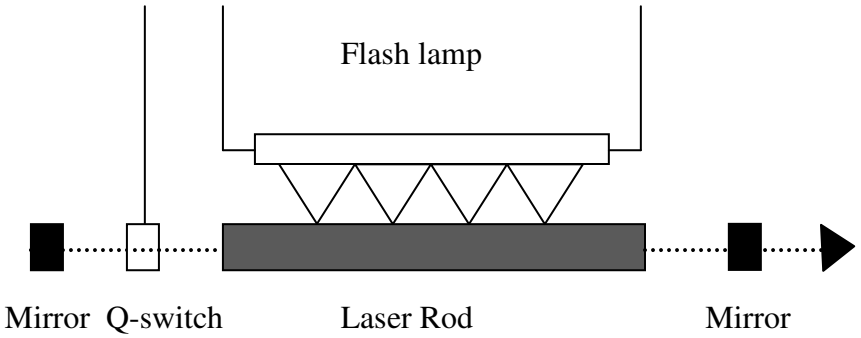

Figure 5 Schematic diagram of Nd:YAG laser

A Nd:YAG laser consists of a flash lamp, laser rod, Q-switch and mirrors. The flash lamp is used as a light pumping source. The optical resonator is a closed cavity with a neodymium-doped yttrium aluminum garnet crystal ($Nd:Y_3Al_5O_{12}$) as a gain medium. Pumping light is absorbed by Nd^{3+} ions in the gain medium and they become excited. These excited ions release photons having the same energy as the laser atomic transition wavelengths. In this process, a photon passes though the lasing medium and when the frequencies of the photon and the medium are equal, the photon gets amplified due to the stimulation of the decay of other ions from the upper state to the lower state. The mirrors are arranged in a way to make the amplified light reflect back into the resonant cavity to increase the amplification.

Nd:YAG lasers are used in LIF measurements because of their consistency, efficiency, compactness and high laser energy production. The fundamental wavelength

for a Nd:YAG laser is 1064 nm, which can be converted to second, third, and fourth harmonic wavelengths.

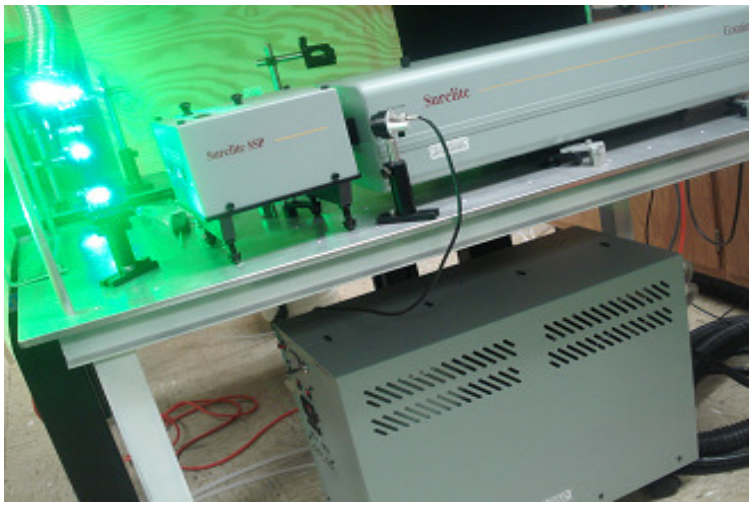

Figure 6 Laboratory used Nd:YAG laser

Table 1 Wavelengths of Nd:YAG laser

Type	Wavelength (nm)	Pulse width (ns)
Fundamental	1064	7
Harmonics – second	532	4 – 6
Third	355	4 – 6
Fourth	266	4 – 6

The fundamental wavelength (1064 nm) is not directly useful for many applications. Different birefringent materials like KDP (Potassium Dihydrogen Phosphate) and KD*P (Potassium Dideuterium Phosphate) can be used to convert the fundamental wavelength to other harmonic wavelengths like 532 nm (second harmonic) and 355 nm (third harmonic) which have two and three times the photon energy of the

fundamental wavelength and are useful for many applications, including dye laser pumping.

Table 2 Energy of fundamental and harmonic wavelengths of Nd:YAG

Wavelength (nm)	energy (mJ)
1064	650
532	280
355	170

Table 3 Specifications of the laboratory Nd:YAG laser (SureLite Laser)

Pulse energy	40 mJ at 355 nm
Pulse duration	4-6 ns
Pulse rate	10 Hz/sec
Energy stability	+/- 2%
Beam diameter	<10 mm
Beam divergence	0.5 mrad
Flash lamp lifetime	$10*10^6$ shots

3.2.2. TUNABLE DYE LASER

Tunable dye lasers are used to change a laser emission wavelength in a given spectral range with the use of organic dyes (Figure 7). Dye molecules absorb pump laser light at one wavelength and reemit at a different wavelength. A dye solution is used as a laser gain medium and circulates within a large reservoir. Organic dyes have broad

fluorescence bands. These bands are excited by a pump laser (Nd:YAG laser) and a laser output wavelength is selected using gratings and prisms. The combination of tunable dye lasers and Laser Induced Fluorescence has been shown to provide high sensitivity for many elements.[98]

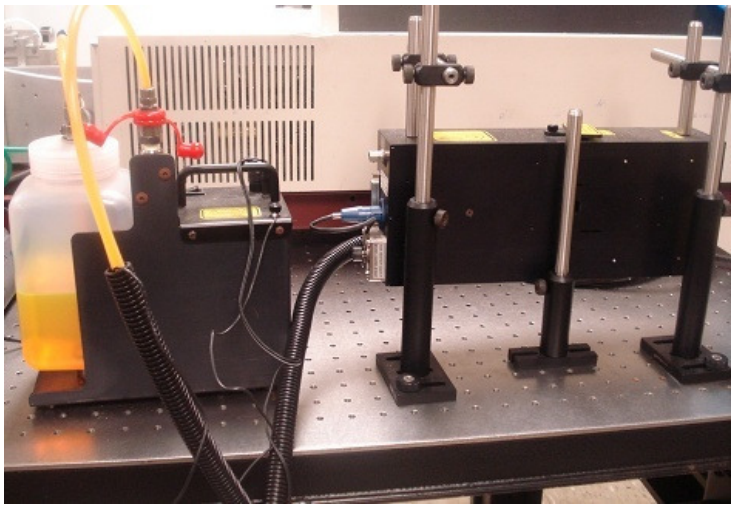

Figure 7 Laboratory used Tunable dye laser

Stilbene (trans-1,2-diphenylethylene) dye has been used in this study as a gain medium (Figure 8). Its molecular formula is $C_{14}H_{12}$ and the molecular weight is 180.24 amu.

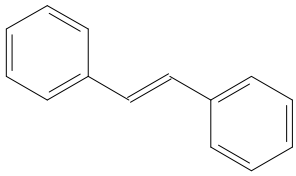

Figure 8 Molecular structure of *trans*-Stilbene

3.2.3. FREQUENCY DOUBLING CRYSTAL

Frequency doubling is the conversion of the fundamental wavelength (1064 nm) to the second-harmonic wavelength (532 nm) by passing the light wave through a non-linear crystal.

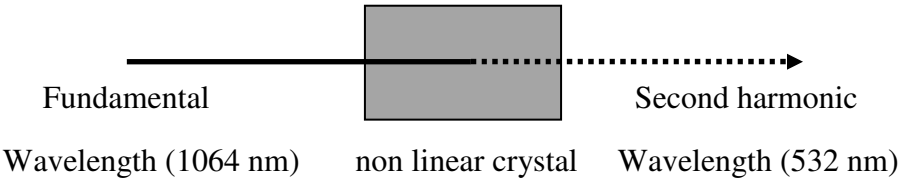

Figure 9 Configuration of Frequency doubling crystal

When passing through the non-linear crystal, the high intensity fundamental wave generates a nonlinear polarization in the material, which provides a new wave at twice the fundamental frequency. The generated wavelength has half of the original wavelength and twice the original frequency. Common frequency doubling crystal materials include lithium niobate ($LiNbO_3$), potassium titanyl phosphate ($KTiOPO_4$), and lithium triborate (LiB_3O_5).

3.2.4. OPTICAL SYSTEMS

Lenses and mirrors of specific focal length are used for focusing and collecting of the laser and fluorescence emissions. Different focal length lens are chosen depending upon the wavelength of the element.

3.2.5. DETECTION SYSTEM

Emitted radiation contains information about the elements that are produced from the sample material. Spectral analysis of the radiation is performed using a grating monochromator (Figure 10). The light reaches a collimating mirror in the monochromator through an entrance slit and is directed towards a diffraction grating. The grating disperses the light by diffracting different wavelengths at different angles. By adjusting the angle of the grating, the desired wavelength can be isolated and directed to a focusing mirror, exit slit and to the Photo Multiplier Tube (PMT) detector.

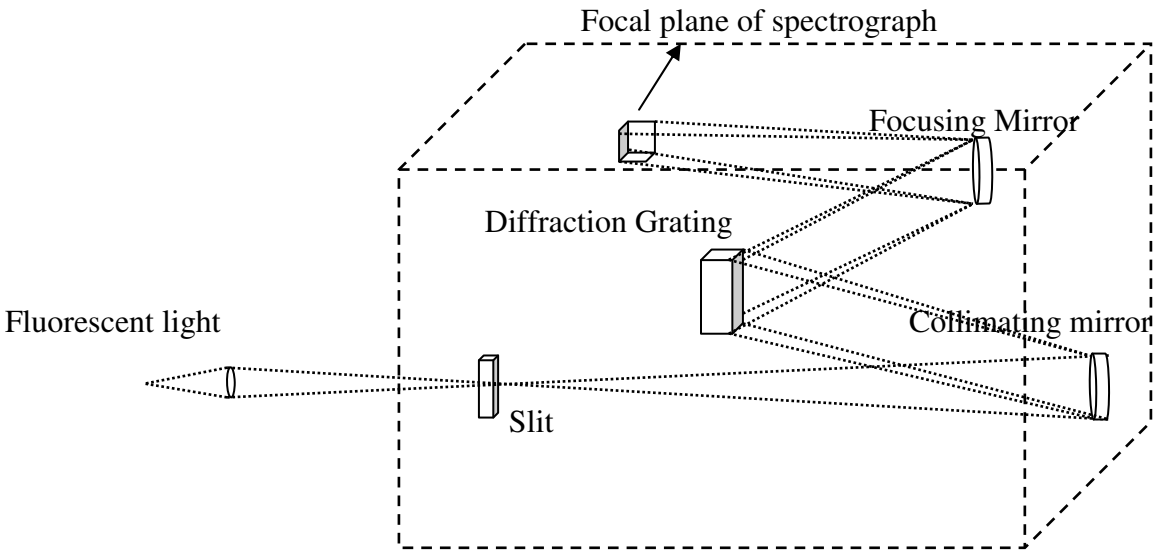

Figure 10 Schematic diagram of Czerny-Turner Grating Monochromator

Table 4 Specifications of Laboratory Czerny Turner monochromator (SpectraPro 275)

Focal length	275 mm
Slit width	Up to 3000 µm
Grating	1200 grooves mm^{-1}
Resolution	0.05 nm
Focal plane	27 mm wide * 14 mm high

PHOTO MULTIPLIER TUBE (PMT)

A Photo Multiplier Tube (PMT) detects light and multiplies a single incident photon to approximately 10^6 electrons. A Photo Multiplier Tube (PMT) consists of a vacuum tube, several dynodes and an anode (Figure 11). The vacuum tube contains a photosensitive material called a photocathode. When a photon strikes the photocathode, it emits a photoelectron due to the photoelectric effect. These photoelectrons are accelerated toward a dynode which produces 2-5 electrons from a single incident electron. When the secondary electrons strike another dynode, additional secondary electrons are produced. These electrons move further into the tube producing additional secondary electrons. All these electrons reach the anode producing an electrical pulse, which can be read by the oscilloscope.

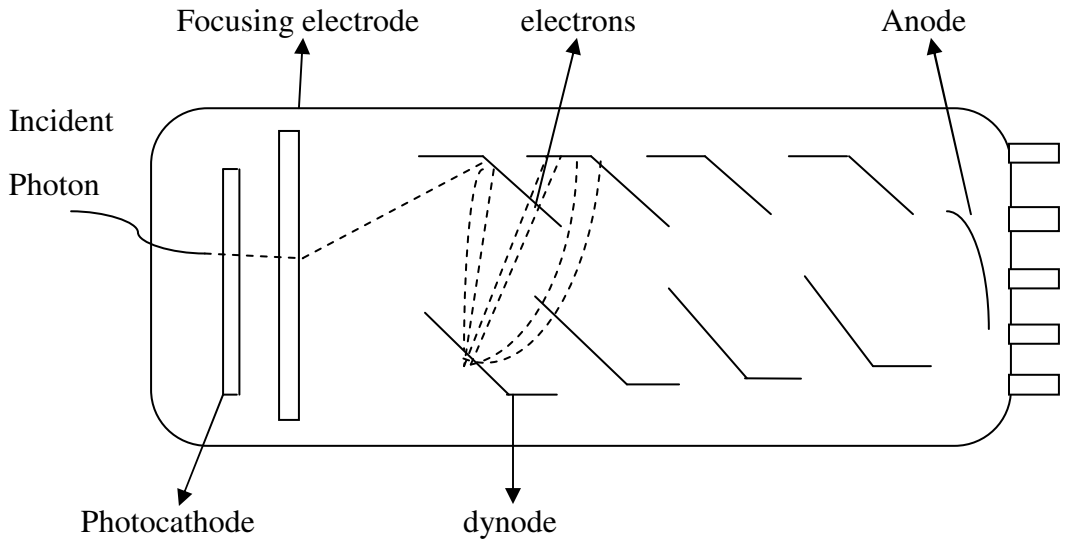

Figure 11 Schematic diagram of Photo Multiplier Tube (PMT)

3.2.6. OSCILLOSCOPE

An oscilloscope is an instrument that converts the waveform of detector signal into an electrical signal and displays it as a function of time (Figure 12). In operation mode, it has a trace line in the middle of the screen, which displays the voltage change with time. The image is controlled by a time base control and a vertical voltage control. The time base control adjusts the scale of the horizontal axis in seconds and the vertical control adjusts the vertical axis in volts. An external trigger transfers an input pulse from the laser source and the signal trace is displayed on a phosphor screen.

Figure 12 Laboratory used Oscilloscope

3.3. INDUCTIVELY COUPLED PLASMA ATOMIC EMISSION SPECTROSCOPY (ICP-AES)

The ICP-AES instrumentation used in this project consists of 3 major parts (Figure 13)

1. Sample introduction
   A. Nebulizer
   B. Spray chamber
2. ICP torch
3. Detector

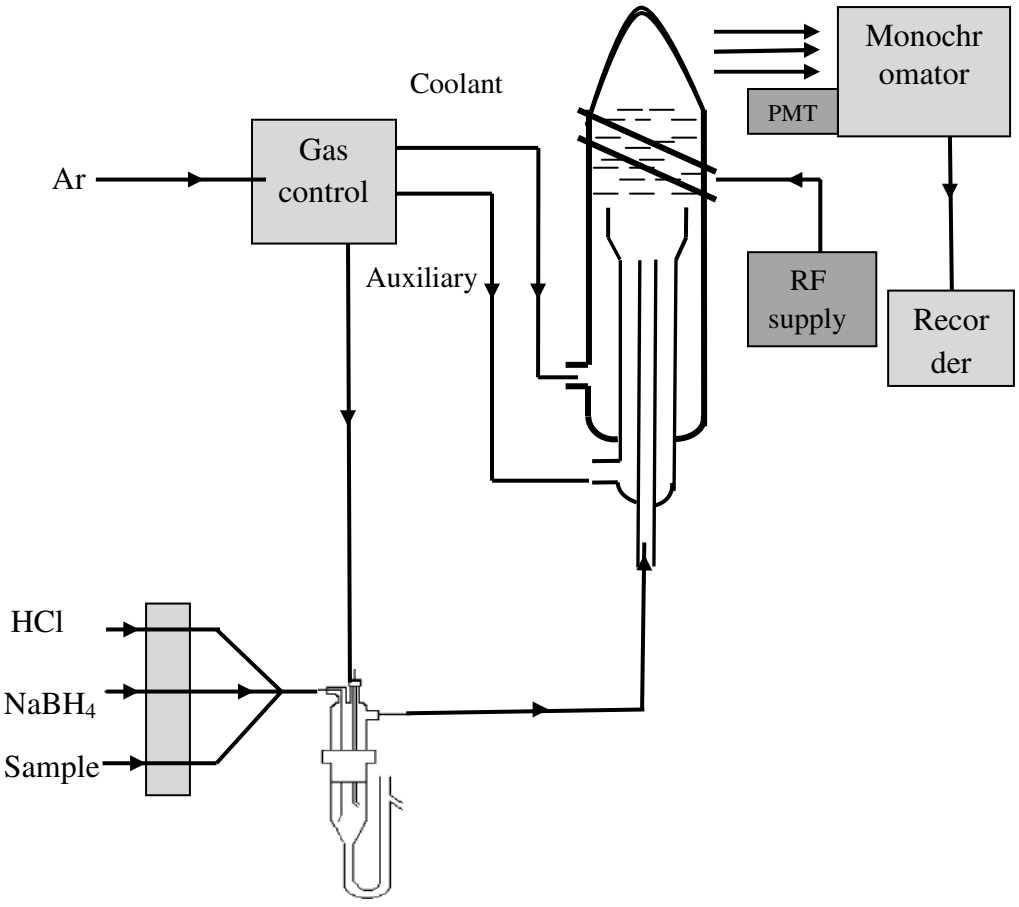

Figure 13 Schematic Diagram of HG-ICP-AES

Figure 14 Laboratory used ICP-AES

3.3.1. SAMPLE INTRODUCTION

Solution nebulization sample introduction includes introduction of the sample into the nebulizer, conversion of the sample into an aerosol and transport of the aerosol into the plasma. In ICP methods, the sample can be introduced in solid, liquid or gaseous forms. The most commonly used nebulizer is the pneumatic nebulizer, which is usually made of glass or polymers to resist highly corrosive samples. Pneumatic nebulizers convert a sample solution into an aerosol by an argon gas flow. The argon gas draws the sample solution through a capillary, which is adjusted in the gas flow to assist the aerosol generation.

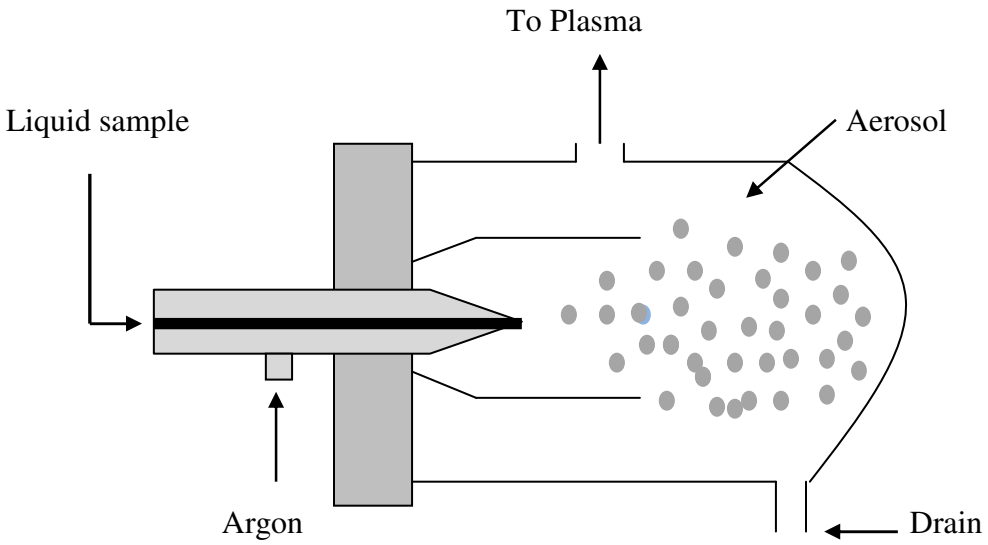

Figure 15 Schematic diagram of pneumatic nebulizer and spray chamber

3.3.2. SPRAY CHAMBER

The spray chamber is located between the nebulizer and the ICP torch and separates the aerosol particles by their size (Figure 15). Only smaller particles are allowed to travel to the plasma while larger particles are trapped and exit through the drain tube of the spray chamber. The spray chamber also smoothes out pulses that may occur due to the peristaltic pump used to deliver the sample solution to the nebulizer.

3.3.3. INDUCTIVELY COUPLED PLASMA (ICP)

The ICP is used as an atomization and excitation source in ICP-AES (Figure 14).[99] The plasma is a type of electrical discharge that contains ions, electrons and atoms. The plasma is formed at atmospheric pressure, has high temperatures, and can be produced by either an electric or magnetic field. Argon gas is the most commonly used gas for plasma formation because it is inert, relatively inexpensive, and easily obtained at high purity.

3.3.4. ICP TORCH

The ICP torch is made of three circular concentric quartz tubes for argon gas flow and sample introduction (Figure 16). Argon gas flows through the outer channel at a flow rate of 7-15 L min^{-1} and enters into the plasma. An auxiliary flow of Ar passes through the middle channel at a rate of 0.5 to 3 L min^{-1}. The nebulizer gas flows through the center channel and is used to inject the sample gas flow into the plasma. In the ICP, the sample gas flows at a rate of 0.1 to 1 L min^{-1}.

An induction coil is wrapped around the top of the quartz torch and is connected to a radiofrequency generator (RF). When RF power (700-1500 watts) is applied to the induction coil, it produces a magnetic field at a radio frequency of 27-40 MHz. When electrons are introduced into the magnetic field, they are accelerated due to induction. These electrons collide with Ar atoms producing secondary electrons. The chain reaction of argon ionization and breakdown inside the plasma is known as an ICP discharge.

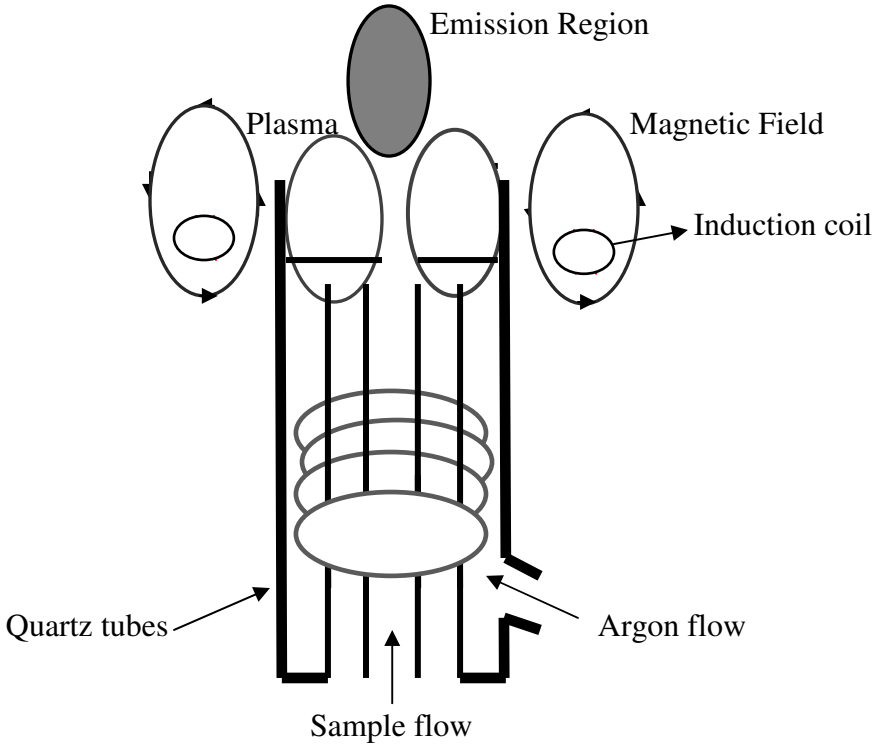

Figure 16 Schematic diagram of the ICP and torch

The analytical observation zone of the ICP is above the torch and the height is adjusted to give the best optical viewing area for maximum sensitivity. Plasma temperatures typically range from 7000-8000 K, which is sufficient to atomize and excite almost all elements.

3.3.5. ATOMIZATION OF SAMPLE IN ICP

Atomization of a sample involves the following steps

1. Sample preparation – samples are usually prepared by dissolving the samples into dilute solutions using acids, bases or microwave digestion techniques.
2. Nebulization – liquid samples are converted into aerosol.
3. Desolvation – water is completely removed from the aerosol particles.

4. Vaporization – dried aerosol particles are converted to gases.
5. Atomization – vaporized solute molecules are converted to atoms.
6. Ionization – atoms are converted to ions due to collisions with electrons.

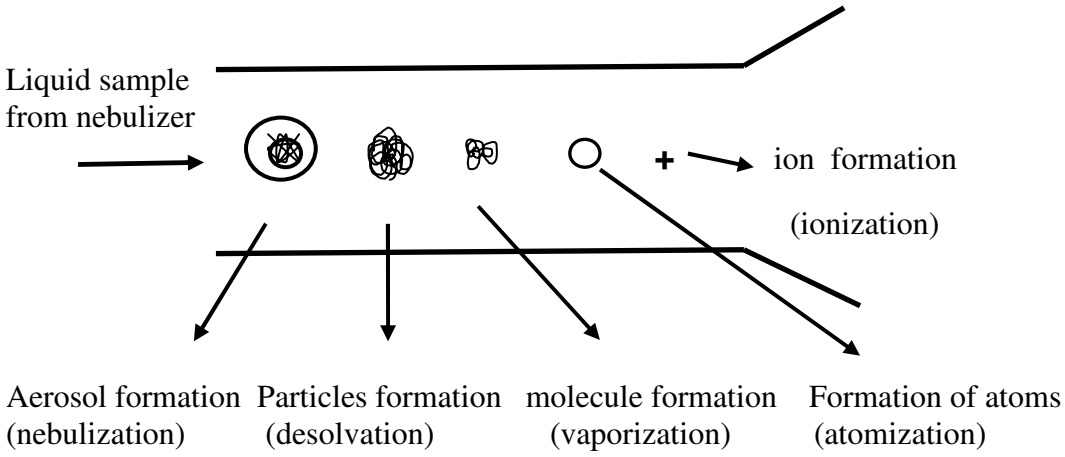

Figure 17 Sample ionization in the plasma

3.3.6. DETECTORS

The emitted radiation from the analytical zone of the plasma is collected for spectroscopic measurement. Radiation is collected by focusing optics and analyzed by a monochromator. The monochromator isolates the desired wavelength and transmits it to the PMT for detection.

Detailed notes on detectors are given in section 3.2.5.

3.4. LASER INDUCED BREAKDOWN SPECTROSCOPY (LIBS)

The LIBS instrumentation used in these studies (Figure 18) consists of

1. Nd:YAG laser
2. Optics for generation of plasma and to direct the laser pulse onto the sample
3. Optics to collect and transport the light to the detector system
4. Detection system consisting of a monochromator and a detector
5. Boxcar and a computer to collect and store the spectrum

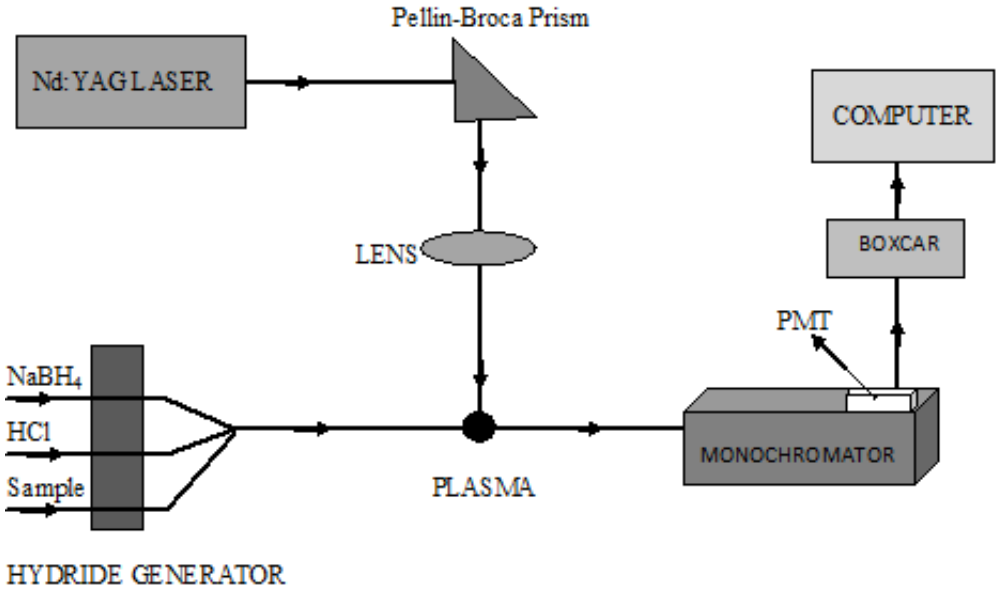

Figure 18 schematic diagram of LIBS

A Nd:YAG pulsed laser (detailed information in section 3.2.1) is used to produce the plasma. A prism directs the laser beam 90^{o} from its initial direction and a lens is used to focus the laser pulse on the sample by quartz optics. The emitted light is collected and

transported to the detection system. In these experiments, one lens is used to produce the plasma and one lens is used to collect and focus the plasma light.

A continuous flow hydride generator (detailed information in section 1.9) is used to convert dissolved metal ions into their hydrides. The radiation emitted from the excited atoms contains information about elements in the sample material. The emitted radiation is quantified by the detection system.

A boxcar gated integrator and averager is a device used to process the incoming detector signal by adjusting different parameters such as the gate delay (t_d), gate width (t_w), sensitivity, and averaging (Figure 19). The gated integrator enhances the signal by avoiding background signals and interferences and averages multiple laser shots to reduce shot to shot variations. The gate width is adjusted to collect the light for a specific period of time, while the gate delay is adjusted to avoid intense plasma background emissions.

Figure 19 Laboratory used Boxcar Integrator

3.4.1. LIBS PLASMA

A laser plasma is an electrically neutral environment that is composed of atoms, ions and free electrons. Depending upon the degree of ionization, plasmas are characterized as weakly ionized plasmas that have a low electron to atom/ion ratios or highly ionized plasmas that have high electron to atom/ion ratio. Most LIBS plasmas are weakly ionized.[100] Laser plasma generation involves photon ionization, electron collision, and secondary electron production. Once the plasma is formed, elements are excited to different energy levels. The plasma usually decays within microseconds after the laser pulse has terminated. Laser intensities of more than 1 Gwatt cm^{-2} are generally required for sample breakdown. The plasma temperature typically ranges from 8000-10,000 K.

Laser plasma generation depends on several factors such as laser wavelength, pulse energy and irradiance. In these studies, the laser wavelengths include the fundamental wavelength of 1064 nm, the second harmonic of 532 nm and the third harmonic of 355 nm. Depending upon these wavelengths, the pulse energies ranged from 10 mJ to 200 mJ. The irradiance (intensity) is typically about 10^{18} photons cm^{-2}.

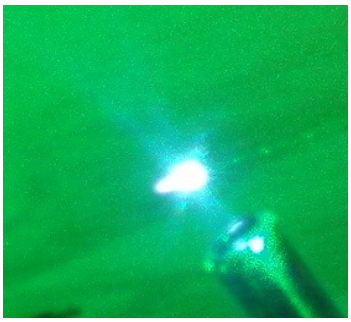

Figure 20 Laboratory produced LIBS plasma

CHAPTER IV

EXPERIMENTAL SECTION

4.1. CHEMICALS AND MATERIALS

The 1.5% (m/v) solution of sodium tetrahydroborate was prepared by combining 2.0% (m/v) of $NaBH_4$ (98%, Sigma-Aldrich, Germany) and 0.4% of (m/v) NaOH (> 98%, Sigma-Aldrich, Germany) and diluting it with de-ionized water. Diluted hydrochloric acid (Pharmco-AAPES, CT, USA) was prepared by diluting the concentrated acid with de-ionized water. The tellurium stock solution (1000 ppm) was prepared by dissolving 2.35 g of sodium tellurite (Na_2TeO_3, Sigma-Aldrich, Germany) in 1 liter of de-ionized water. Other standard solutions for Sn (Spex, NJ, USA), As (Sigma-Aldrich, Switzerland), Bi (Sigma-Aldrich, Switzerland), Ni (Sigma-Aldrich, Switzerland), Ge (Sigma-Aldrich, Switzerland), Zn (Sigma-Aldrich, Switzerland), and Co (Sigma-Aldrich, Switzerland) were commercially available in a concentration of 1000 ppm. All the working solutions were prepared by diluting the stock solution with de-ionized water. The glassware was thoroughly cleaned with 1% hydrochloric acid and de-ionized water prior to use. All the reagents and working solutions were prepared freshly each day.

4.2. EXPERIMENTAL SET UP FOR LIF

The Nd:YAG laser produces light pulses at 355 nm (third harmonic wavelength) of about 40 mJ $pulse^{-1}$ at a rate of 10 Hz with 5 ns duration. To produce the desired wavelength of 214 nm, the 355 nm radiation is first converted to 428 nm using a tunable dye laser and Stilbene 420 laser dye (Exciton, NJ, USA). A frequency doubling crystal is used to reduce the wavelength into half by doubling its frequency, to convert the 428 nm radiation to 214 nm. The laser light passes through several optics and into the flame atomizer to cause excitation of metal atoms. The laser excited atoms emit fluorescence light that is directed towards the monochromator by a 25 cm focal length lens. The monochromator (Czerny-Turner spectrograph) isolates the desired wavelength and directs it to the photomultiplier tube (PMT). The photomultiplier tube converts the light signal into an electrical signal and is recorded by an oscilloscope. The excitation wavelengths used for tellurium and tin were 214.275 nm and 286.333 nm, and the emission wavelengths were 238.325 nm and 317.505 nm, respectively.

Table 5 Experimental Conditions used for LIF

LASER	Q-switched Nd:YAG laser
Wavelength	355 nm
Pulse width	10 ns
Repetition rate	10 Hz
Energy used	40 mJ
LENS	Quartz made, 25 cm focal length
PMT voltage	-1200 V
DETECTION SYSTEM	
Spectrophotometer	SpectraPro 275, MA, USA
Grating	Czerny-Turner, 1800 grooves mm-1
Slit width	1500 µm
Slit height	4 mm
HYDRIDE GENERATION	Rainin, dynamax RP-1, CA, USA
HCl Concentration	10%
$NaBH_4$ + NaOH Concentration	1.5% + 0.4%

Table 6 Experimental conditions used for Te and Sn in LIF

Conditions	**LIF (Te)**	**LIF (Sn)**
Concentrations of solution (ppb)	0.01, 0.03, 0.1, 0.5, 1, 3	0.01, 0.03, 0.1, 0.5, 1, 3
Absorption Wavelength (nm)	214.275	286.333
Emission Wavelength (nm)	238.325 and 238.576	317.505
PMT voltage	-1200 V	-1200 V
Averaging	256	256

4.3. EXPERIMENTAL SET UP FOR ICP-AES

The ICP instrument used in these studies was an ARL 3410 ICP with mini torch (ARL, CA, USA). The reference line for the instrument was an argon line at 355.43 nm. For hydride generation, high purity Argon gas was used to purge the hydride gas toward the plasma. The spectral data were recorded using commercial software (ICP Manager, Micro-Active Australia Pvt. Ltd, Australia). For hydride generation studies, a continuous flow hydride generator with a peristaltic pump (Rainin, dynamax RP-1, CA, USA) was used.

Table 7 Experimental conditions used for the ICP-AES measurements

RF power	1 kW
Frequency of RF generator	21.31 MHz
Coolant gas flow rate	8.5 L min-1
Auxiliary gas flow rate	0.8 L min-1
Sample gas flow rate	0.8 L min-1
Monochromator	Czerny-Turner spectrograph 1800 groves mm^{-1}
Integration time	3 s
Hydride Generator	Rainin, dynamax RP-1, CA, USA
HCl Concentration	0.55 M
$NaBH_4$ + NaOH Concentration	1.5% + 0.4%

4.4. EXPERIMENTAL SET UP FOR LIBS

A Nd:YAG pulsed laser (Continuum, SureLite SLII-10) produces laser pulses at a 10 Hz repetition rate, and 5 ns duration. To produce the plasma, the fundamental wavelength of 1064 nm is converted to the second harmonic wavelength 532 nm by using birefringent materials like KDP (Potassium Dihydrogen Phosphate) or KD*P (Potassium Dideuterium Phosphate).

The laser beam is directed 90^{o} to its initial direction by using a quartz prism. Quartz optics are used to focus the laser pulse onto the gas sample, to collect the spark light, and to transport it to the detection system.

A continuous flow hydride generator with a peristaltic pump (Rainin, dynamax Rp-1, CA, USA) was used to convert the dissolved metal ions into their hydrides. The three channel peristaltic pump mixes the HCl, $NaBH_4$, and sample solutions and generates the metal hydride, which is directed into the path of the laser beam. The high plasma temperature of 10,000 K excites the atoms which emit photons. The radiation emitted from the plasma contains information about elements in the plasma that are produced from the sample material. The emitted radiation is directed towards the monochromator.

Spectral analysis is performed using a monochromator (Czerny-Turner Spectrograph). The monochromator isolates the desired wavelength and directs it to the photomultiplier tube (PMT). The photomultiplier tube detects the light signal and converts it to an electrical signal. The electrical signal is processed by the boxcar and is recorded by using commercial software (SRS, Palo Alto, CA, USA).

Table 8 Experimental Conditions used for LIBS

LASER	Q-switched Nd:YAG laser
Wavelength	532 nm and 355 nm
Pulse width	10 ns
Repetition rate	10 Hz
Energy used	40 mJ to 200 mJ
LENS	Quartz made
PMT Voltage	-1200 V
BOXCAR	
Time delay	700 ns to 3 µs
Gate width	1 µs to 3 µs
Average	30 to 1000
DETECTION SYSTEM	
Spectrophotometer	SpectraPro 275, MA, USA
Grating	Czerny-Turner, 1800 grooves mm^{-1}
Slit width	10 µm to 100 µm
HYDRIDE GENERATOR	Rainin, dynamax RP-1, CA, USA
HCl Concentration	10%
$NaBH_4$ + NaOH Concentration	1.5% + 0.4%

Table 9 Experimental conditions used for Arsenic, Tellurium, and Tin

Conditions	**As**	**Te**	**Sn**
Concentrations of metal solution (ppm)	1, 2, 3, 4, 5	1, 2, 3, 4, 5	1, 2, 3, 4, 5
HCl Concentration	10%	10%	10%
$NaBH_4$ + NaOH Concentration	1.5% + 0.4%	1.5% + 0.4%	1.5% + 0.4%
Emission Wavelength	197.197 nm	214.275 nm	270.651 nm
PMT voltage	-1200 V	-1200 V	-1200 V
Slit Width	100 µm	50 µm	50 µm
Time Delay	3 µs	1 µs	2 µs
Gate Width	3 µs	2 µs	3 µs
Averaging	300	300	300

Table 10 Transition probabilities of atomic transitions used in this study[101]

Wavelength (nm)	**Element**	**Energy levels (Cm^{-1})**	**gA (10^8/sec)**
214.275	Te I	0-46653	5.8
238.325	Te I	4707-46653	6.4
238.576	Te I	4751-46653	8.2
286.333	Sn I	0-34914	5.3
317.505	Sn I	3428-34914	3.2
235.484	Sn I	1692-44145	11.0
224.605	Sn I	0-44509	2.6
283.999	Sn I	3428-38629	21.0
242.949	Sn I	3428-44576	29.0
270.651	Sn I	1692-39259	2.3
231.604	Ni I	8394-51558	59.0
234.554	Ni I	0-42621	5.5
213.856	Zn I	0-46745	19.0
206.200	Zn II	0-48481	92.0
265.118	Ge I	1410-39118	26.0
209.426	Ge I	1410-49144	9.2
204.377	Ge I	1410-50323	5.0
237.862	Co II	3350-45379	158.0
236.379	Co II	4029-46321	166.0
197.197	As I	0-50694	5.0

CHAPTER V

RESULTS AND DISCUSSION

5.1. LASER INDUCED FLUORESCENCE

5.1.1. Optimal conditions for HG-LIF

In the LIF studies, it was first necessary to determine the excitation wavelength of the metal hydrides. By measuring the signal levels at different wavelengths, the absorption wavelengths for tellurium (Te) and tin (Sn) were determined separately. These wavelengths corresponded to strong absorptions shown in table 10. The efficiency of continuous flow hydride generation depends on several factors including reactant concentrations, solution flow rates and gas flow rates.[88] The dependence of the fluorescence intensity of tellurium on the concentrations of hydrochloric acid and sodium tetrahydroborate were evaluated in the range of 5% to 20% (v/v) and 0.5% to 2.0% (m/v), respectively. For the acid, the Te fluorescence signal increased linearly with increasing acid concentration (Fig. 21a), while the fluorescence signal increased up to 1.5% and then decreased with changing $NaBH_4$ (Fig. 21b). These levels are similar to those reported previously for Te and other elements.[40] Concentrations of 1.5% of borohydride and 10% of acid were chosen for further experiments because higher concentrations led to higher background.

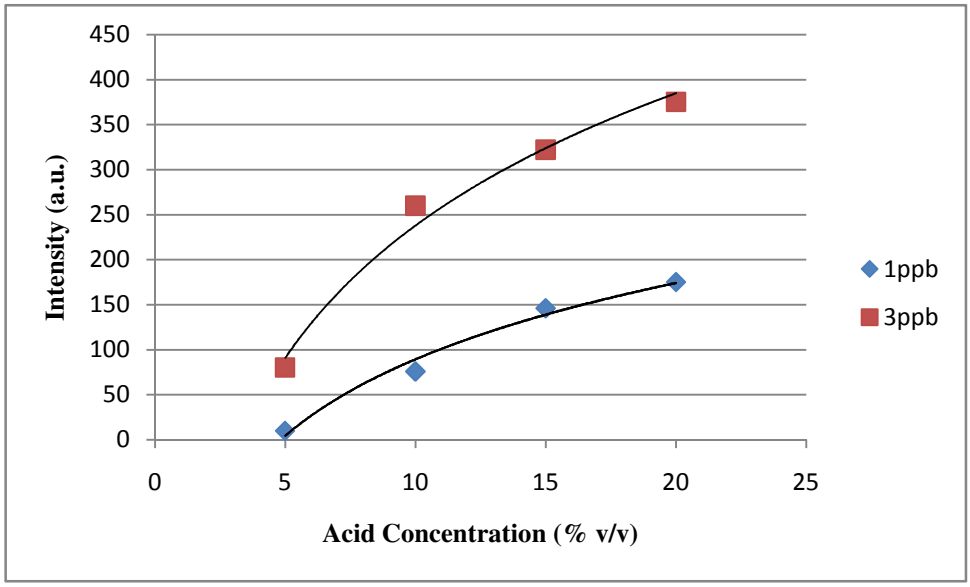

Figure 21a Influence of hydrochloric acid concentration on fluorescence intensity of Te

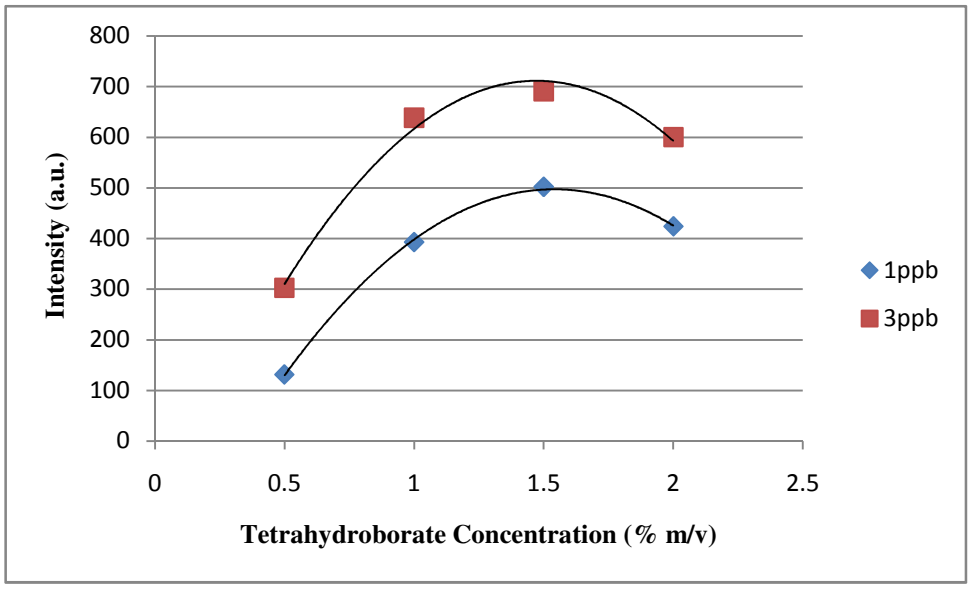

Figure 21b Influence of sodium tetrahydroborate concentration on fluorescence intensity of Te

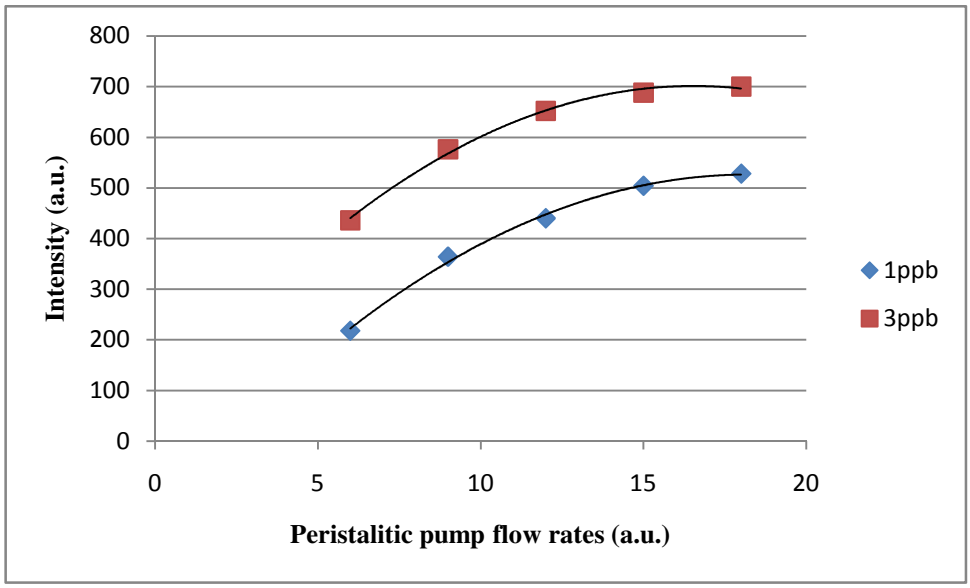

Figure 21c Influence of Peristaltic pump flow rates on Fluorescence Intensity of Te

Figure 21c shows the influence of the peristaltic pump flow rates on the observed fluorescence intensity. The signal increased with an increase in flow rate. The corresponding volumetric flow rates for the solutions are shown in Table 11.

Table 11 Peristaltic pump flow rates of Acid, $NaBH_4$ and Sample

Pump flow rate (a.u.)	HCl (mL min^{-1})	$NaBH_4$ (mL min^{-1})	Sample (mL min^{-1})
5	3.2	3.2	5.3
10	6.2	6.2	9.7
15	8	8	14
20	12	12	18

In this system, helium is used to carry the volatile hydride towards the atomizer and hydrogen is used to support the flame used for atomization of the hydrides. The hydrogen and helium flow rates were also optimized.

Figure 21d shows the influence of the slit width on the fluorescence intensity. The fluorescence signal increased with the slit width up to 1500 µm and then decreased.

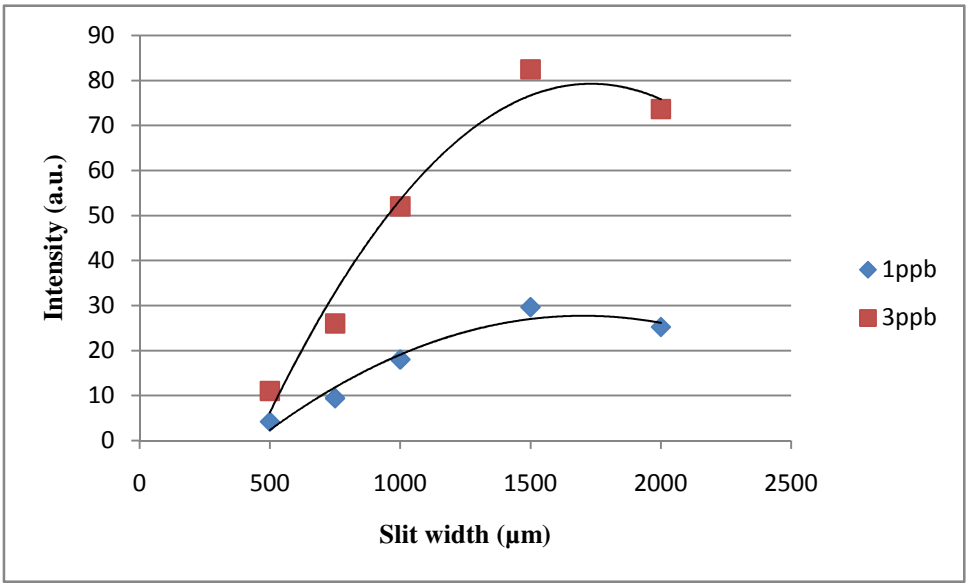

Figure 21d Influence of monochromator slit width on Fluorescence Intensity of Te

Table 12 Optimal conditions for HG-LIF

Parameters	**Te**	**Sn**
Acid Concentration	10% (v/v)	10% (v/v)
Hydroborate Concentration	1.5% (m/v)	2.0% (m/v)
Peristaltic pump flow rate	15 a.u.	15 a.u.
Monochromator slit width	1500 µm	1500 µm

Figure 22 show the power dependence of the fluorescence signal. Initially the fluorescence signal increased with laser energy in a linear way, but after a certain point there was no change in the signal. This point indicates that the fluorescence excitation is saturated. After this point the signal varied only slowly with laser energy. This is important because LIF measurements conducted with laser energies above the saturation point depend on weakly on the laser power. This has the result of reducing the effects of laser energy variations as a source of noise on the LIF measurements.

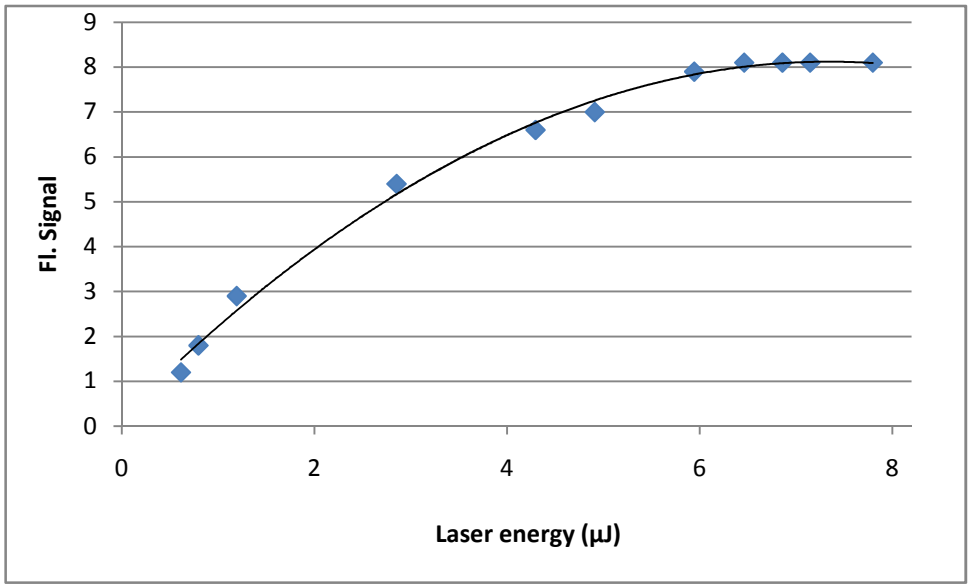

Figure 22 Fluorescence of Te as a function of laser energy

5.1.2. Calibration and Analytical figures of merit

In order to determine the sensitivity and limit of detection of the HG-LIF approach, calibration curves were performed and typical curves for Te and Sn are shown in Figures 23 and 24. It was observed that the fluorescence signal increased in a linear

way with the increase in Te concentration. The signal was stabilized by washing the sample tube each time for at least 3 minutes after changing the solutions.

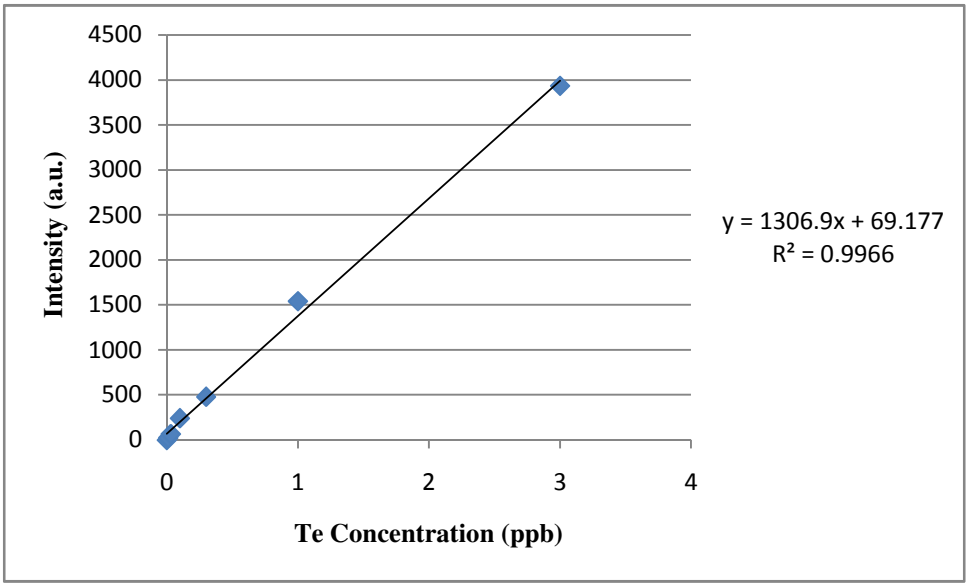

Figure 23 Calibration curve for Te-HG-LIF

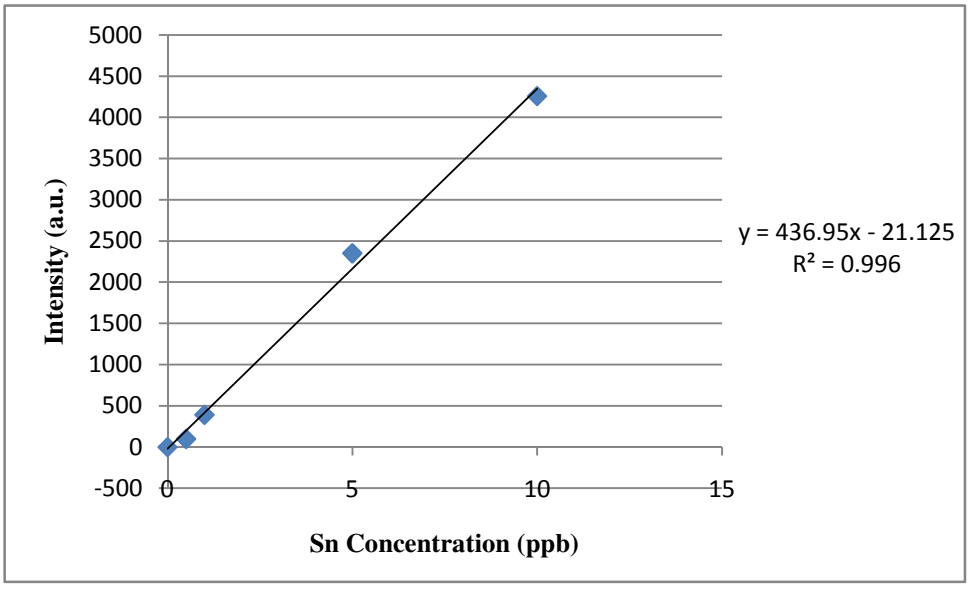

Figure 24 Calibration curve for Sn-HG-LIF

At high concentrations the fluorescence emission could exceed the detector capacity. Neutral Density (ND) filters were used to limit the amount of light reaching the detector (for concentrations more than 1 ppb). The ND filters are used to reduce light intensity that is caused due to the higher concentrations of the analyte. When using these filters, the actual signal intensity is determined by multiplying the observed intensity with the attenuation factor of the filter. In this experiment, ND 1 and ND 2 filters were used.

Table 13 Attenuation factors of the ND filters at different wavelengths

Wavelength (nm)	**ND 2 filter**	**ND 1 filter**
300.914	191.87	8.54
317.505	161.97	8.08
472.500	120.75	8.29
406.000	135.69	7.96
364.000	135.65	7.83

By using the optimum conditions, several calibration curves were performed. The results obtained showed a Limit of Detection of 0.008 ppb (8 ppt) for tellurium and 0.07 ppb for tin. Table 14 shows the analytical figures of merit obtained for the calibration curves.

Table 14 Analytical figures of merit for HG-LIF

Analytical Figures	**Te**	**Sn**
Linear range (ppb)	0.01 to 10	0.1 to 10
Limit of Detection (ppb)	0.008	0.07
Limit of Quantification (ppb)	0.02	0.2
Relative Standard Deviation (%)	0.01	0.1

Table 15 Comparison of LOD of HG-LIF with previous techniques

Method	**Te (ppb)**	**Sn (ppb)**
Flame AA	30[102]	150[102]
HG-AAS	0.2[65]	0.25[66]
HG-AFS	0.76[40]	0.04[63]
ICP-OES	2[102]	2[102]
ICP-MS	0.0008[95]	0.0006[65]
HG-LIF*	0.008	0.07

The LOD obtained here for Te (0.008 ppb) is lower than that reported previously by several commercial approaches, but not as low as the ICP-MS approach. The LOD obtained for Sn (0.07 ppb) is lower than that reported by several other approaches, comparable to Sn-HG-AFS approach and higher than the ICP-MS approach. These data indicate that the HG-LIF approach is one of the more sensitive methods for trace measurements of these elements.

5.2. INDUCTIVELY COUPLED PLASMA ATOMIC EMISSION SPECTROSCOPY (ICP-AES)

For comparison purposes, it was of interest to study several elements by ICP-AES. These elements included bismuth, tin, tellurium, nickel, zinc, germanium and cobalt. All these elements were studied by ICP-AES using solute nebulization and bismuth, tin, and tellurium by both nebulization and hydride generation sample introduction techniques.

5.2.1. BISMUTH

5.2.1.1. Calibration curve

By using a 5 second measurement integration time, a calibration curve for bismuth was performed in a concentration range of 1 ppm to 4 ppm at different Bi emission wavelengths.

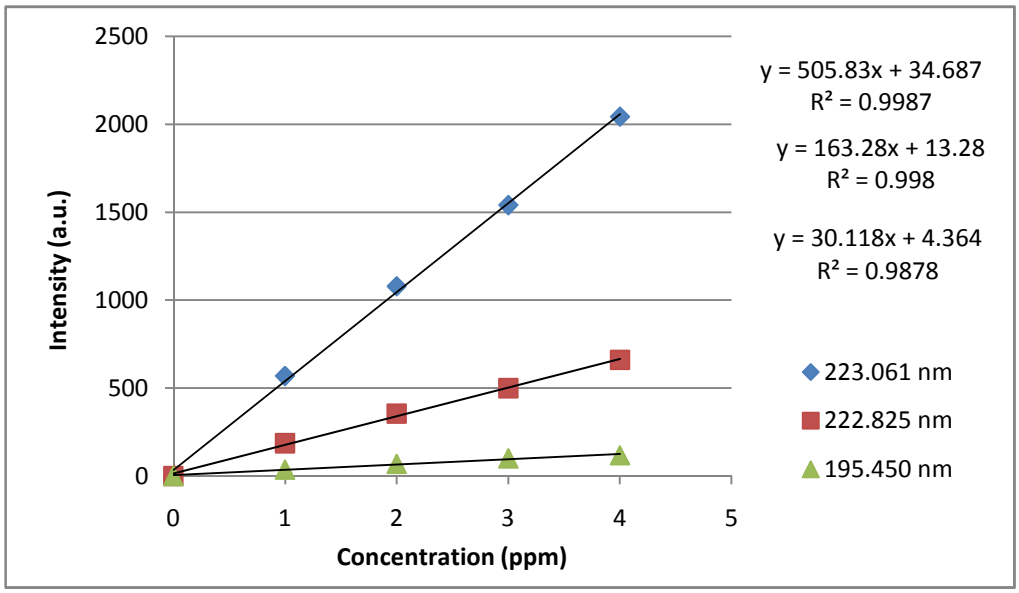

Figure 25a Calibration curve for Bi-ICP-AES

The limit of detection was calculated using the standard deviation of 16 blank measurements and the slope of the calibration curve. The LODs are given in table 16.

Table 16 LODs of Bismuth at different emission wavelengths

Wavelength (nm)	**LOD (ppb)**
222.825	20
223.061	50
195.389	200

By using 1.5% (m/v) sodium tetrahydroborate and 0.75 M hydrochloric acid, a calibration curve for bismuth was performed using HG-ICP-AES at 222.825 nm with a measurement integration time of 5 sec.

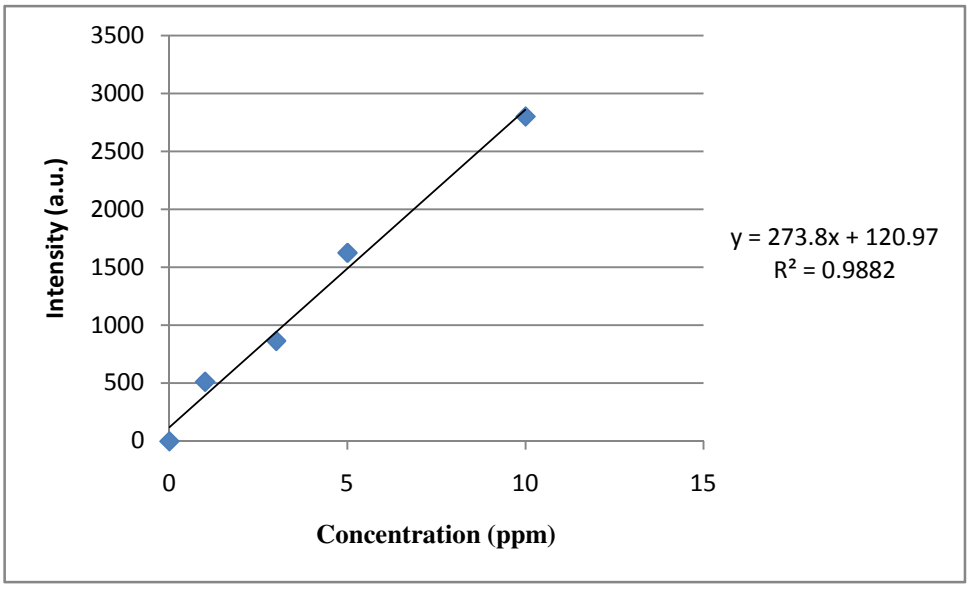

Figure 25b Calibration curve for Bi-HG-ICP-AES

The obtained LOD of 0.1 ppm using HG-ICP-AES with HG was slightly higher than the LOD of ICP-AES without HG which is only 20 ppb. The addition of thiourea and ascorbic acid to the sample solution of HG to mask possible interferences did not show the effects as described in the literature.[36] After conducting several experiments, it was concluded that the HG approach did not improve the results for ICP-AES measurements using this instrument.

Table 17 Comparison of LOD's of Bi-ICP-AES with other techniques[102]

Method	**Bi (ppb)**
Flame AA	30
Flame AA-HG	0.03
GFAA	0.05
ICP-OES	1
ICP-MS	0.0006

The LOD obtained here (20 ppb) for Bi is lower than that reported for the Flame AA, but not as low as has been reported previously for other commercial approaches.

5.2.2. TIN

5.2.2.1. Calibration curve

By using a 5 second measurement integration time, a calibration curve for tin was performed. The concentrations used were 0.1, 0.5, 1, 2, 3, and 5 ppm.

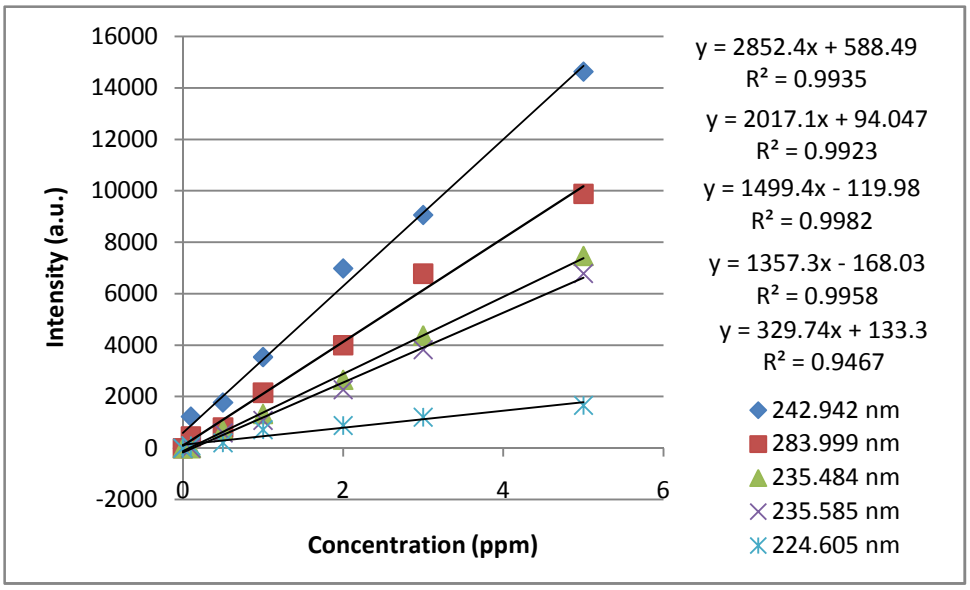

Figure 26a Calibration curve for Sn-ICP-AES

The limit of detection was calculated by using the standard deviation of 16 blank measurements and the slope of the calibration curve. The LODs are shown along with literature value, for other methods in table 18 and 19.

Table 18 LOD's of Tin at different wavelengths

Wavelength (nm)	**LOD (ppb)**
235.585	6
235.484	19
224.605	14
283.999	22
242.949	10

Using 1.5% w/v sodium borohydride and 0.055 M hydrochloric acid, a calibration curve was performed using measurements at 235.585 nm with an integration time of 5 sec. The plot is shown in Figure 26b.

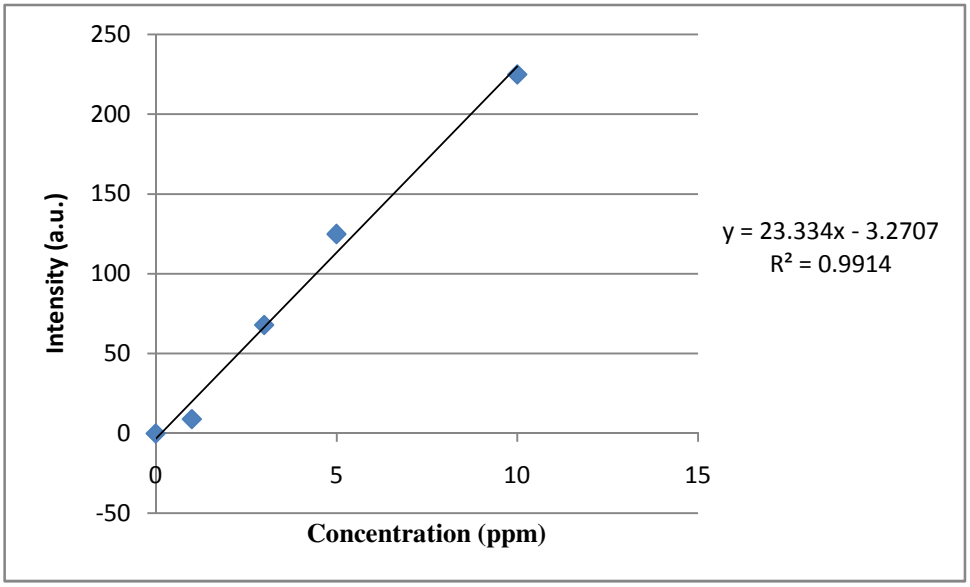

Figure 26b Calibration curve for Sn-HG-ICP-AES

The results obtained with hydride generation sample introduction for tin are not as good compared to results obtained without hydride generation. The LOD of 1 ppm seen

with HG is higher than the 6 ppb obtained without HG. After conducting several experiments, it was concluded that the current system is not improved by using HG for Sn measurements.

Table 19 Comparison of Sn-ICP-AES with other techniques

Method	**Sn (ppb)**
Flame AA	150[102]
GFAA	0.1[102]
ICP-AES	2[102]
HG-AAS	0.25[66]
HG-AFS	0.04[63]
ICP-MS	0.006[65]

The LOD obtained here (6 ppb) for Sn is lower than that reported for the Flame AA, comparable to a previously reported ICP-AES approach, but not as good as that reported previously for other approaches.

5.2.3. TELLURIUM

5.2.3.1. Calibration curve

By using a 5 second measurement integration time, a calibration curve for tellurium has been performed by the ICP-AES approach at a wavelength of 238.386 nm. The concentrations of Te used were 1, 3, 5, 10 and 20 ppm.

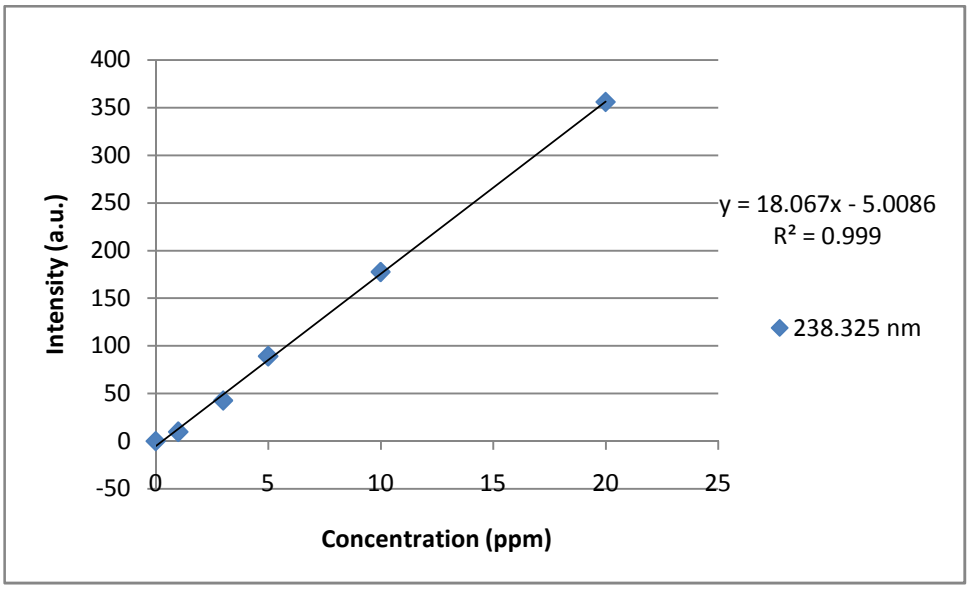

Figure 27a Calibration curve for Te-ICP-AES

The limit of detection was calculated by using the standard deviation of 16 measurements of the blank and the slope of the calibration curve. The LOD obtained was 3 ppb.

By using 1.5% m/v sodium borohydride and 0.55 M hydrochloric acid, a calibration curve was performed by the HG ICP AES approach at 238.386 nm with a measurement integration time of 5 sec.

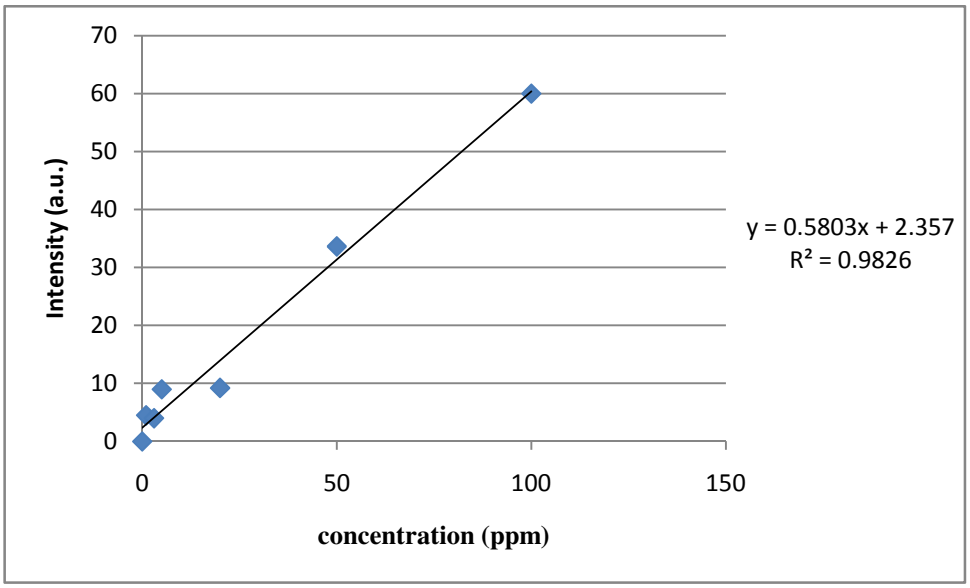

Figure 27b Calibration curve for Te-HG-ICP-AES

The limit of detection obtained with hydride generation for Te is not as good as that obtained without hydride generation technique. The LOD of 2 ppm was observed with HG, while it was 3 ppb without HG. After conducting several experiments it was concluded that the current laboratory system is not improved by using HG for Te measurements.

Table 20 Comparison of Te-ICP-AES with other techniques

Method	**Te (ppb)**
Flame AA	30[102]
GFAA	0.1[102]
HG-AAS	0.2[65]
HG-AFS	0.76[40]
ICP-OES	2[102]
ICP-MS	0.0008[102]

The LOD obtained here (3 ppb) for Te is lower than that reported for the Flame AA, comparable to that reported by other ICP-AES techniques, but not as low as the other HG approaches.

5.2.4. Response of plasma torch to different acid and borohydride concentrations

The reaction of 4 M HCl and sodium tetrahydroborate solution was very strong and made the plasma unstable, probably because of the large amount of H_2 produced. Concentrations of 2 M and 1 M HCl also produced the same effect, where as 0.05 M HCl generated a good signal with a moderate reaction (Table 21).

Table 21 Response of plasma torch to different acid and borohydride concentrations

HCl (M)	**$NaBH_4$% + NaOH%**	**Reaction**	**Torch status**
4 M	2% + 0.4%	very strong	torch off
2 M	2% + 0.4%	Strong	torch off
1 M	2% + 0.4%	Strong	torch off
0.5 M	2% + 0.4%	Moderate	Torch on but no change in signal
0.05 M	2% + 0.4%	Moderate	Torch on and good signal

5.2.5. NICKEL

5.2.5.1. Calibration curve

By using a 5 second measurement integration time, a calibration curve for nickel was performed. The concentrations used were 0.5, 1, 2, 3, and 4 ppm.

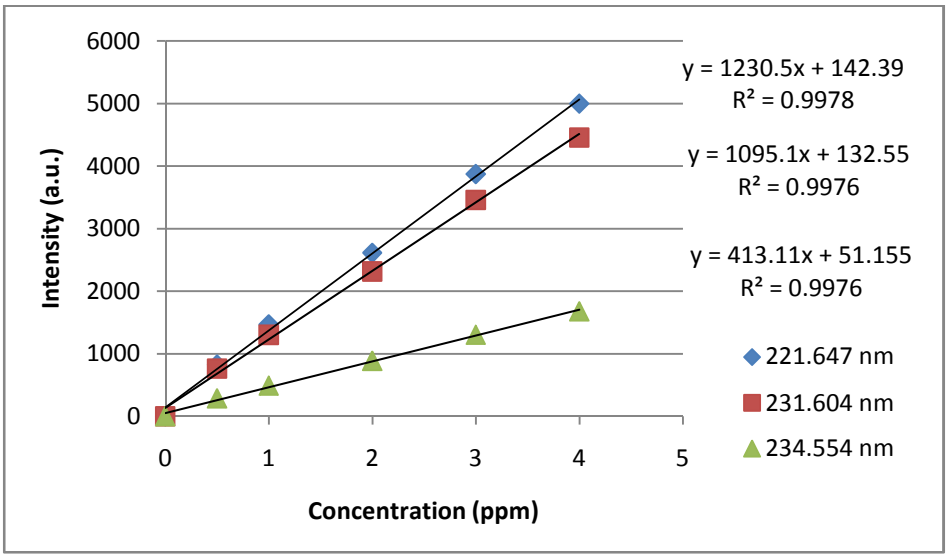

Figure 28a Calibration curve for Ni-ICP-AES

The limit of detection was calculated by using the standard deviation of 16 measurements of the blank and the slope of the calibration curve. The LODs obtained are shown along with reported values for other analytical methods (table 22 and 23).

Table 22 LOD's of Nickel at different wavelengths

Wavelength (nm)	**LOD (ppb)**
221.647	7
231.604	8
234.554	10

Table 23 Comparison of LOD of Ni-ICP-AES with other techniques

Method	**Ni (ppb)**
Flame AA	6[102]
ICP-OES	0.5[102]
ICP-MS	0.0036[83]

The LOD obtained for nickel was found to be 7 ppb, which is comparable to Flame AA but higher than that for other reported methods.

5.2.6. ZINC

5.2.6.1. Calibration curve

By using a 5 second measurement integration time, a calibration curve for zinc has been performed at two different wavelengths. The concentrations used were 0.5, 1, 2, 3 and 4 ppm.

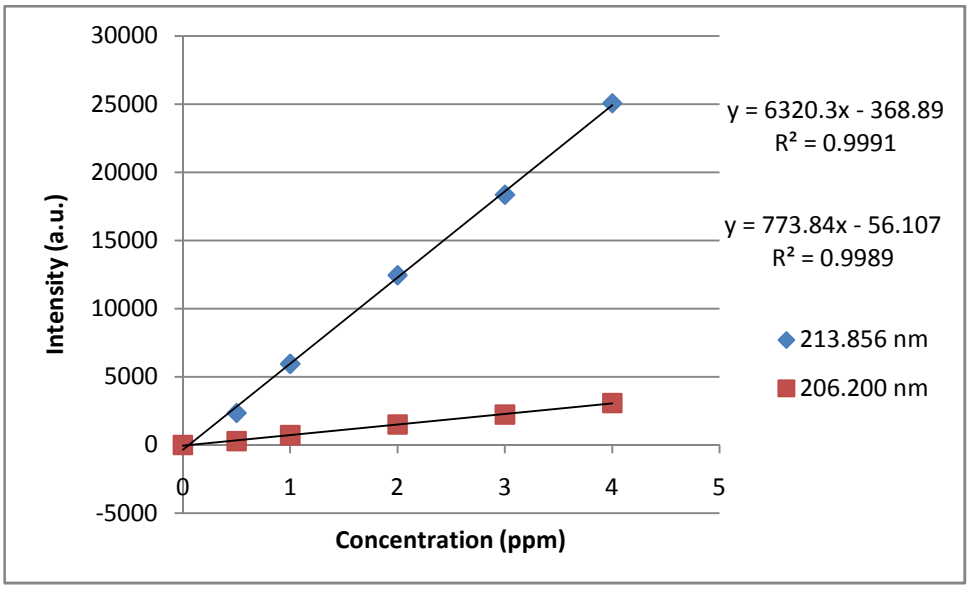

Figure 29a Calibration curve for Zn-ICP-AES

The limit of detection was calculated by using the standard deviation of 16 measurements of the blank and the slope of the calibration curve.

Table 24 LOD's of Zinc at different wavelengths

Wavelength (nm)	**LOD (ppb)**
213.856	2
206.200	9

Table 25 Comparison of Zn-ICP-AES with other techniques[102]

Method	**Zn (ppb)**
Flame AA	1.5
GFAA	0.02
ICP-AES	0.2
ICP-MS	0.0003

The LOD obtained here (2 ppb) for Zn is comparable to that reported for flame AA, but not as low as that reported for ICP-AES, GFAA or ICP-MS.

5.2.7. GERMANIUM

5.2.7.1. Calibration curve by using ICP-AES

By using a 5 second measurement integration time, a calibration curve for germanium has been performed at two different wavelengths. The concentrations used were 0.5, 1, 2, 3, and 4 ppm.

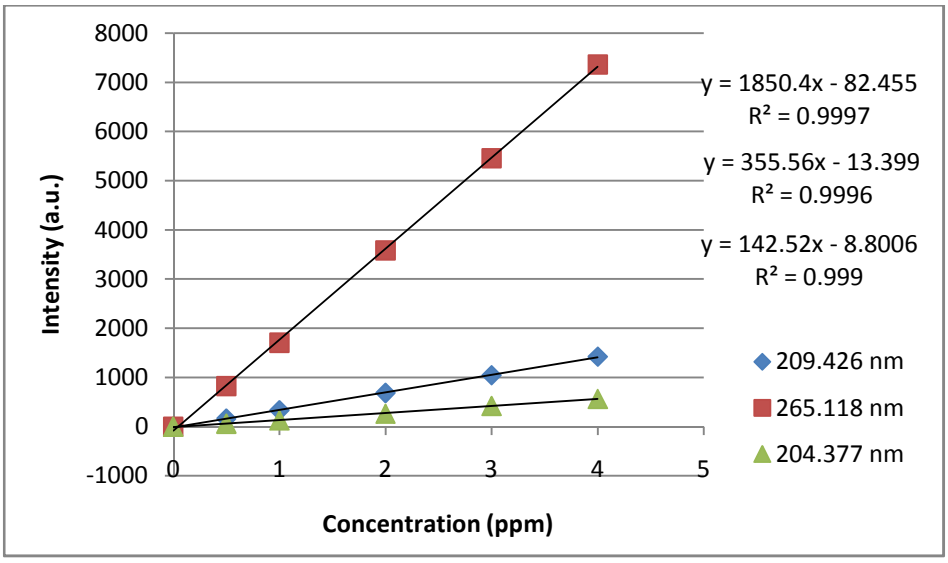

Figure 30a Calibration curve for Ge-ICP-AES

The limit of detection was calculated by using the standard deviation of 16 measurements of the blanks and the slope of the calibration curve.

Table 26 LOD's of Germanium at different wavelengths

Wavelength (nm)	**LOD (ppb)**
265.118	10
209.426	4
204.377	60

Table 27 Comparison of Ge-ICP-AES with other techniques

Method	**Ge (ppb)**
Flame AA	300[102]
HG-AFS	0.43[74]
ICP-AES	1[102]
ICP-MS	0.0005[102]

The LOD obtained here (4 ppb) for Ge is lower than that reported for the Flame AA, comparable to that reported by other ICP-AES techniques, but not as low as other approaches.

5.2.8. COBALT

5.2.8.1. Calibration curve

By using a 5 second measurement integration time, a calibration curve for cobalt has been performed. The concentrations used were 1, 3, 5, and 10 ppm.

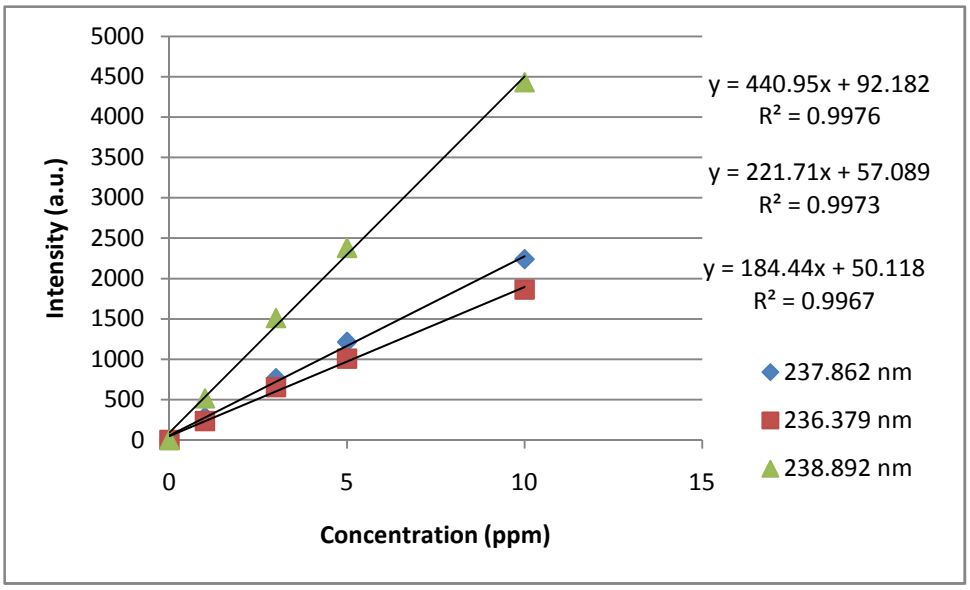

Figure 31 Calibration curve for Co-ICP-AES

The limit of detection was calculated by using the standard deviation of 16 measurements of the blank and the slope of the calibration curve.

Table 28 LOD's of Cobalt at different wavelengths

Wavelength (nm)	**LOD (ppb)**
237.862	20
236.379	8
238.892	16

Table 29 Comparison of Co-ICP-AES with other techniques[102]

Method	**Co (ppb)**
Flame AA	9
GFAA	0.15
ICP-AES	0.2
ICP-MS	0.0009

The LOD obtained here (9 ppb) for Co is comparable to that reported for Flame AA, but higher than that for previously reported approaches.

5.2.9. Detection of elements in a standard solution using ICP-AES

A diluted solution (2 ppm) was prepared from a commercial standard (20 ppm, SPEXcertiprep, NJ, USA) and subjected to ICP-AES measurements. The obtained values are shown in table 30 with uncertainties. These results indicate that the method can be used to provide accurate results at these levels. Similar measurements were not performed with HG-ICP-AES because of the relatively poor sensitivity of the approach.

Table 30 elements and their uncertainties found in standard solution

Element	Concentration found (ppm)	Uncertainty (+/-)
Bi	1.8	0.96
Sn	2	0.23
Te	1.9	0.59
Ni	2	0.32
Zn	1.74	0.98
Ge	1.92	0.68

5.2.10. Comparison of ICP-AES and HG-ICP-AES

Hydride Generation is expected to have an efficiency of nearly 100%, and under proper conditions almost the entire sample should enter the plasma. By comparison, nebulizer efficiency is approximately 2%, and most of the sample is carried to the waste. Due to its high efficiency, HG is expected to be many times more sensitive than comparable measurements using a nebulizer. However in these studies, the sensitivity and LODs were as much as 1000 times higher using HG with ICP-AES as compared to ICP-AES with solution nebulization.

Table 31 Comparison of LOD of ICP-AES and HG-ICP-AES

Method	**Te (ppb)**	**Sn (ppb)**
ICP-AES	3	6
HG-ICP-AES	1000	1000

This suggests that the HG system may not have been interfaced efficiently to the ICP system. This may be due to

1. Several metals being analyzed by HG that might cause memory effects.
2. Argon gas was used for plasma generation. When HG was coupled to ICP-AES, the production of hydrogen caused the plasma to become unstable during analysis and the HG efficiency may have been less then optimum.
3. During the transport of the metal hydride to the torch, most of it gets deposited as a residue and only a small amount of sample reaches the plasma.

Due to several problems with the ICP-AES during the project, it was necessary to switch to another Spectroscopy technique called Laser Induced Breakdown Spectroscopy.

5.3. LASER INDUCED BREAKDOWN SPECTROSCOPY

Laser Induced Breakdown Spectroscopy measurement techniques for Tellurium, Tin, and Arsenic have been studied to evaluate their utility for trace measurements. Different parameters like the boxcar gate width (t_w), gate delay (t_d), and the monochromator slit width have been investigated to optimize the conditions for measurements by LIBS. The gate delay and gate width are adjusted to avoid background noise and interferences. In general, delayed gate times and moderate gate widths are used for good signal integration.

5.3.1. STUDIES USING 355 nm LASER

5.3.1.1. TELLURIUM

5.3.1.1.1. Study of different parameters

Different parameters such as the boxcar gate width, gate delay, and averaging were studied. Figures 32a, 32b, and 32c show a set of spectra that demonstrate the change in the Te spectrum at 214.275 nm with changes in these parameters. The results indicate that a smaller gate width, smaller gate delay and larger slit width allow more noise and lower emission peak intensity. The largest peak intensity combined with a low background was achieved at 2 µs gate width, 1 µs gate delay, and 50 µm slit width.

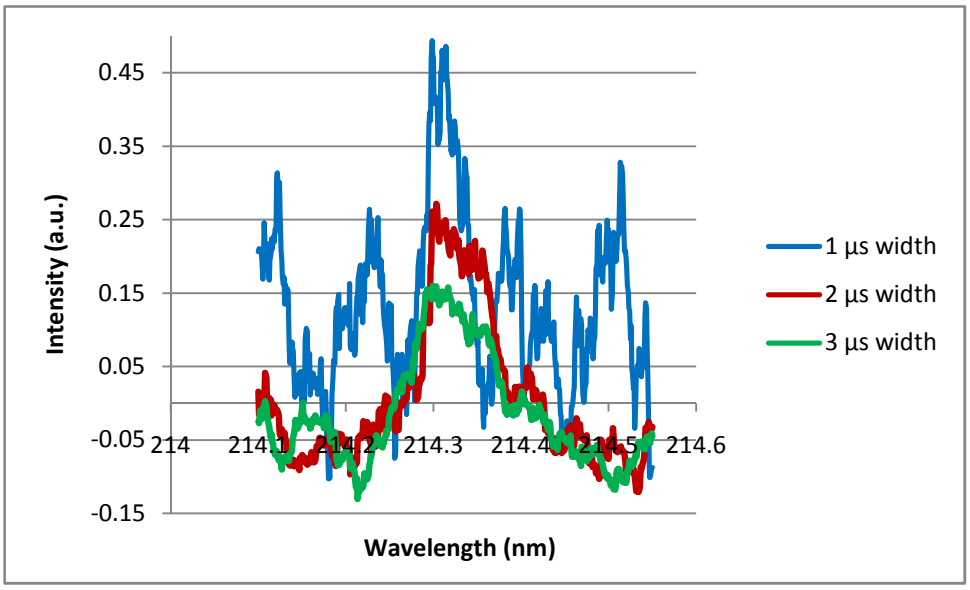

Figure 32a Te emission spectra at different gate widths (1µs delay, 50µm slit width, 300 avgs)

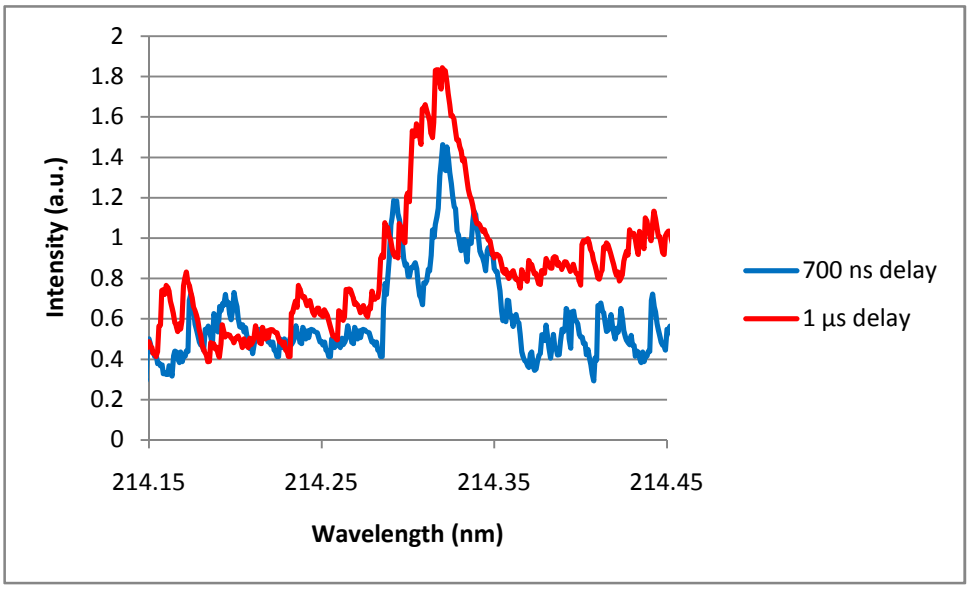

Figure 32b Te emission spectra at different time delays (2 µs gate width, 50 µm slit width, 300 avgs)

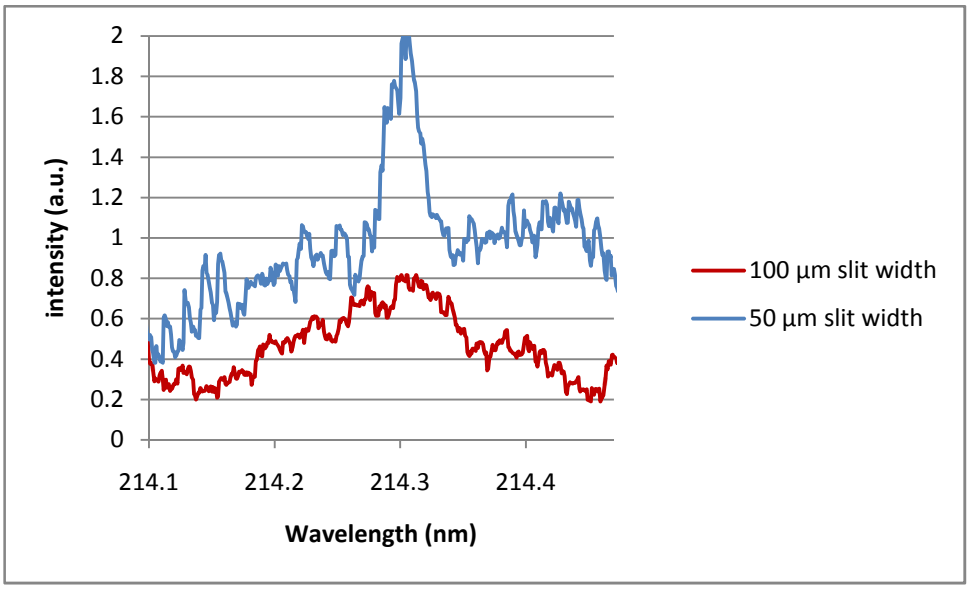

Figure 32c Te emission spectra at different detector slit widths (1 µs delay, 2 µs gate width, 300 avgs)

5.3.1.1.2. Wavelength selection

By using the optimum gate width (2 µs), gate delay (1 µs), monochromator slit width (50 µm), signal average (300), and sensitivity (10 mV/V), the wavelength of 214.3 nm was determined to be the maximum emission wavelength for Te. Shown in Figure 32d is an emission spectrum for Te by HG-LIBS.

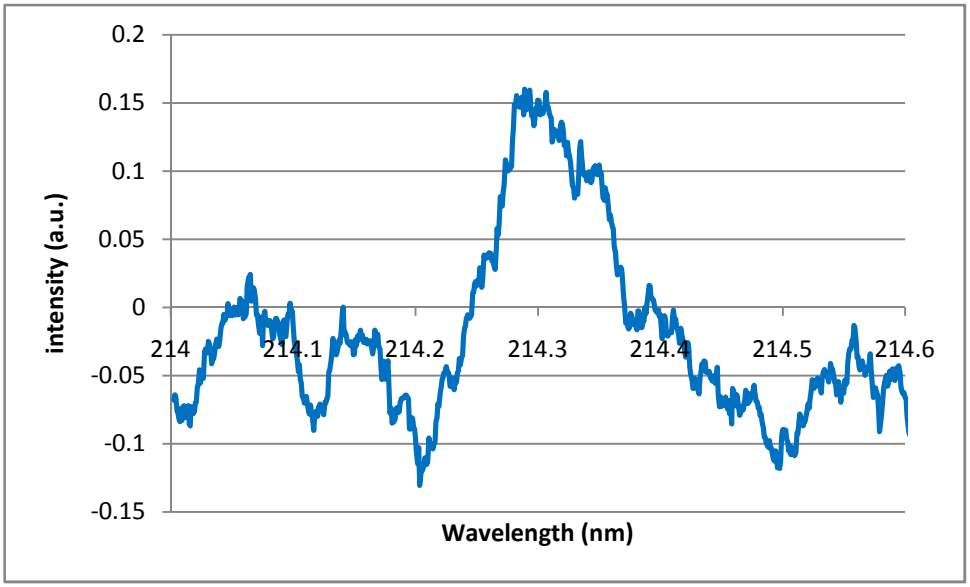

Figure 32d Te emission spectrum (1µs delay, 2 µs width, 50 µm slit width, 300 avgs)

5.3.1.1.3. Calibration and analytical figures of merit

A calibration curve was performed by using the above mentioned optimum conditions at 214.3 nm. To avoid contamination, the measurements were taken in ascending order of concentrations and the system was flushed for 3 minutes between every measurement.

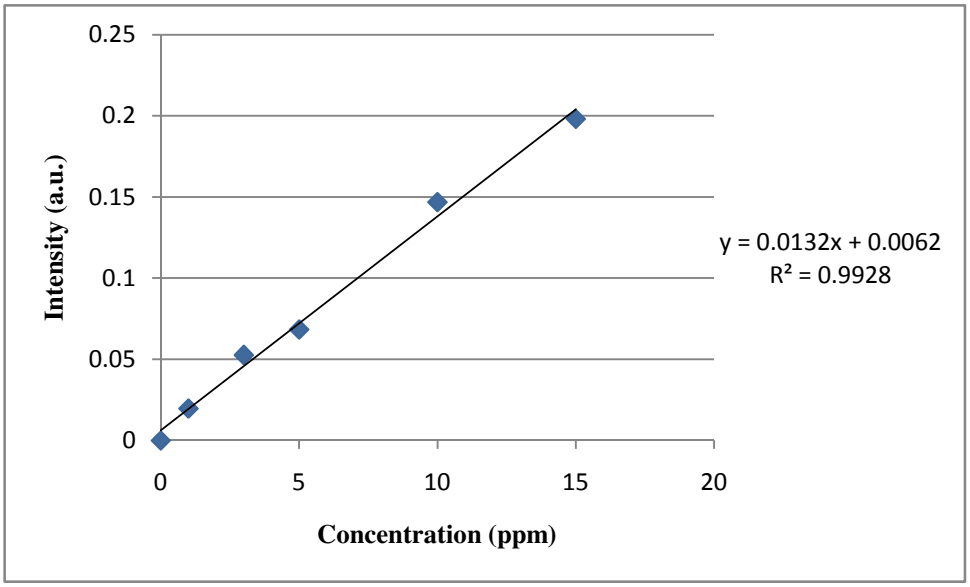

Figure 32e Calibration curve of tellurium at 214.3 nm (1 µs delay, 2 µs width, 50 µm slit width, 300 avgs)

The limit of detection was 1 ppm. A summary of the analytical figures of merit is shown in table 32.

5.3.2. STUDIES USING 532 nm LASER

5.3.2.1. ARSENIC

5.3.2.1.1. Study of different parameters

Several experimental parameters were evaluated for their effect on Arsenic measurements by HG-LIBS. Figures 33a and 33b show the Arsenic emission spectra near 197.3 nm at different gate widths and monochromator slit widths. The results indicate that a smaller gate width and a larger slit width lower the overall peak intensity.

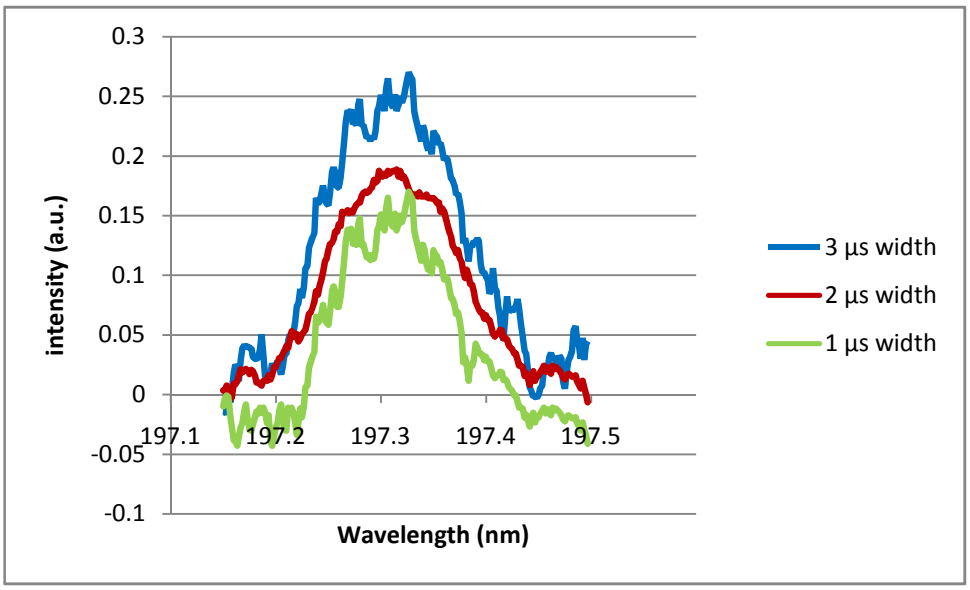

Figure 33a As emission spectra at different gate widths (3 µs delay, 30 µm slit width, 300 avgs)

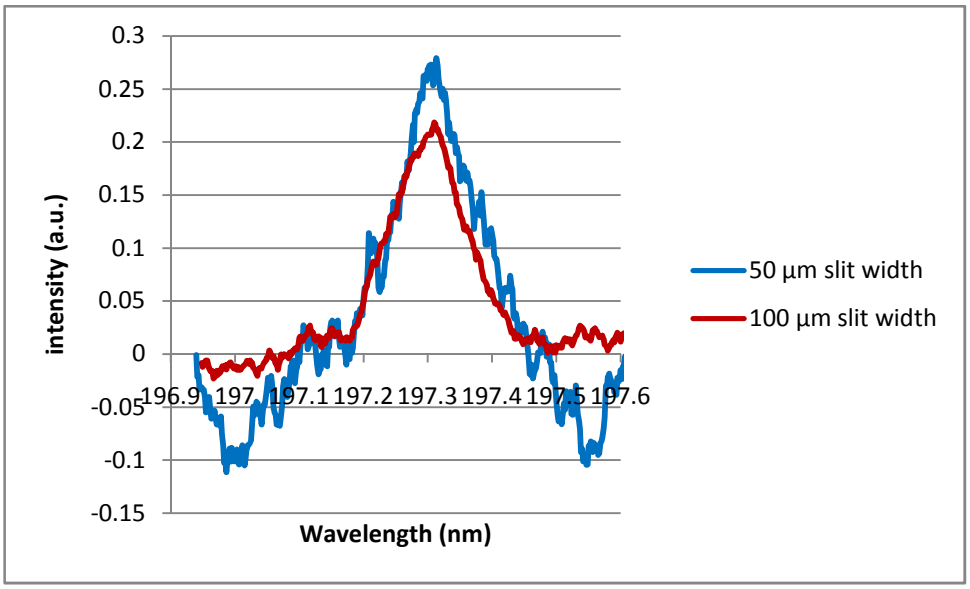

Figure 33b As emission spectra at different detector slit width (3 µs delay, 3 µs gate width, 300 avgs)

5.3.2.1.2. Wavelength selection

By using the optimum experimental conditions, several As emission spectra were measured near the emission wavelength of 197.3 nm. A typical spectrum is shown in Figure 33c.

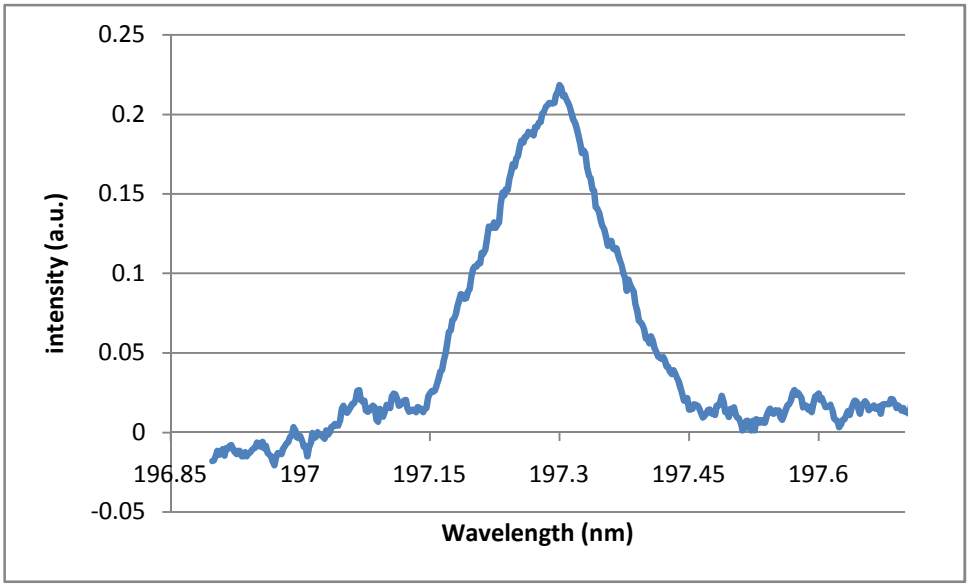

Figure 33c As emission spectrum (3 µs delay, 3 µs width, 30 µm slit width, 300 avgs)

5.3.2.1.3. Calibration and Analytical figures of merit

A calibration curve for As was performed by using the optimum conditions of a gate width of 3 µs, a gate delay of 3 µs, and a monochromator slit width of 50 µm at 197.3 nm. To avoid contamination, the measurements were taken in ascending order of concentrations and the system was flushed for 3 minutes between every concentration.

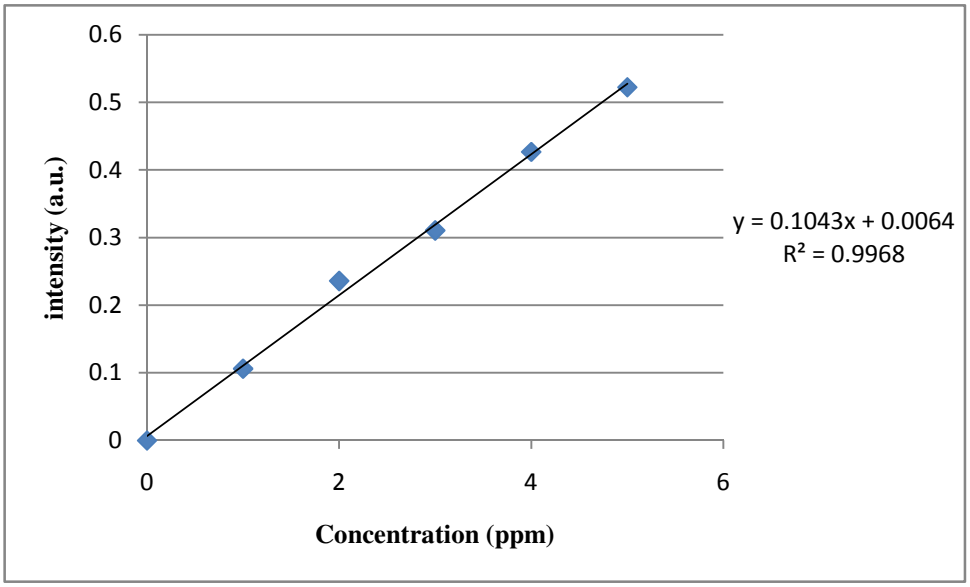

Figure 33d Calibration curve for arsenic at 197.3 nm (3 µs delay, 3µs width, 30 µm slit width, 300 avgs)

The detection limit was 1 ppm. A summary of the analytical figures of merit is given in table 32.

5.3.2.2. TIN

5.3.2.2.1. Study of different parameters

Several experimental parameters were studied for tin measurements by HG-LIBS. Figures 34a and 34b show the tin emission spectra at different boxcar gate width and gate delay. The results indicate that a smaller gate width and smaller gate delay allow more noise and lower overall peak intensity.

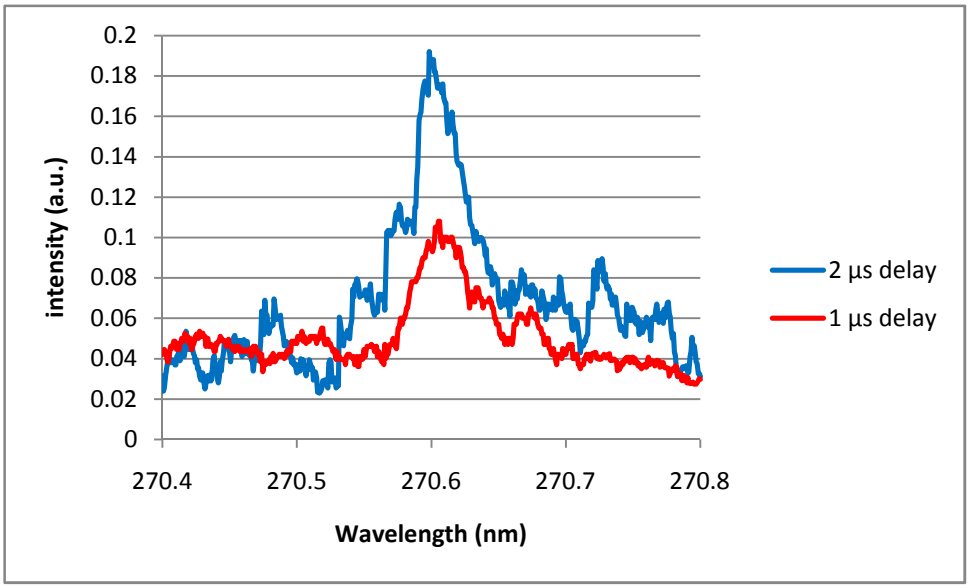

Figure 34a Sn emission spectra at different delays (3 µs gate width, 50 µm slit width, 300 avgs)

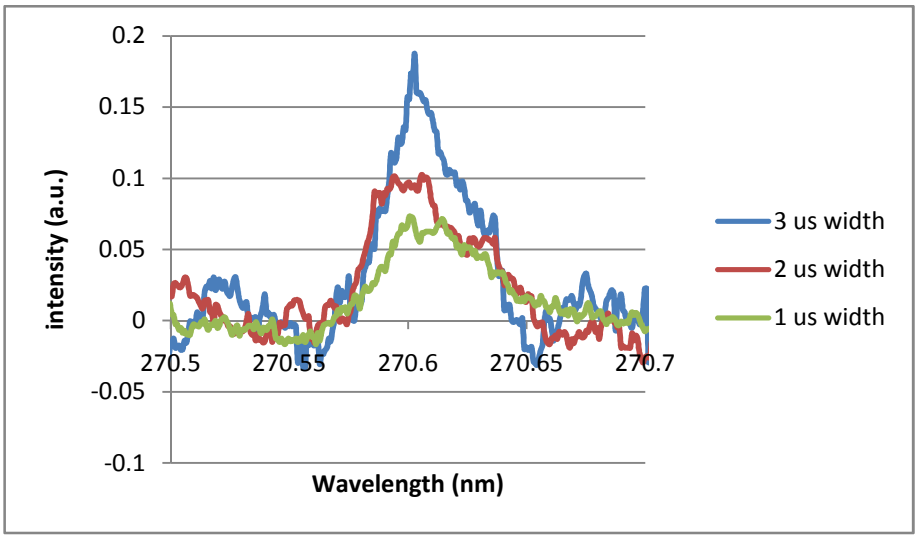

Figure 34b Sn emission spectra at different gate widths (2 µs delay, 50 µm slit width, 300 avgs)

3.2.2.2. Wavelength selection for Tin

By using the optimum experimental conditions, tin emission spectra were recorded near a wavelength of 270.65 nm, as shown in figure 34c.

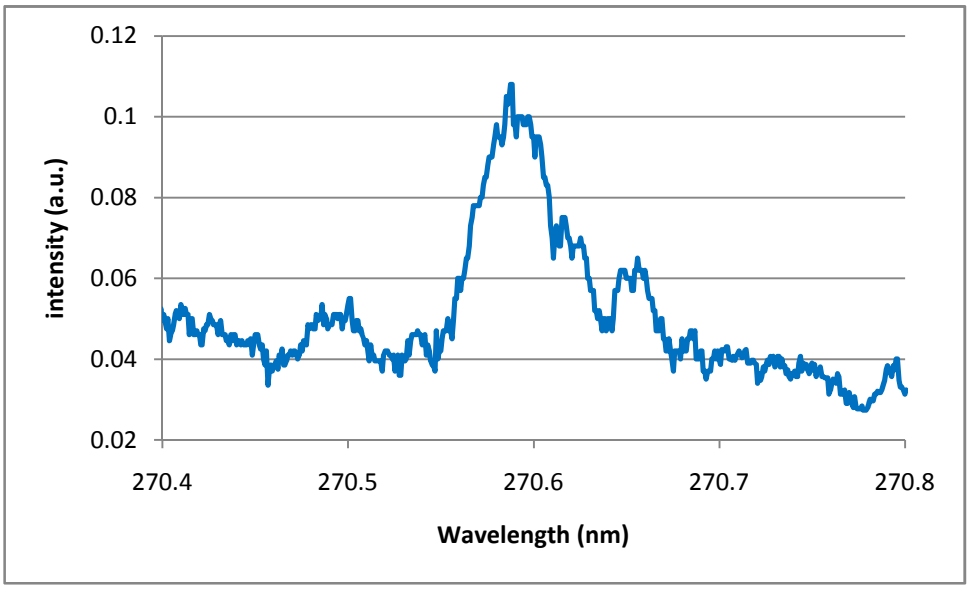

Figure 34c Sn emission spectrum (2 µs delay, 3 µs gate width, 50 µm slit width, 300 avgs)

5.3.2.2.3. Calibration and Analytical figures of merit

A calibration curve was performed by using the optimum conditions, including a gate width of 3 µs, a gate delay time of 2 µs, and monochromator slit widths of 50 µm at 270.65 nm. To avoid contamination, the measurements were taken in ascending order of concentrations and the system was flushed for 3 minutes between every measurement.

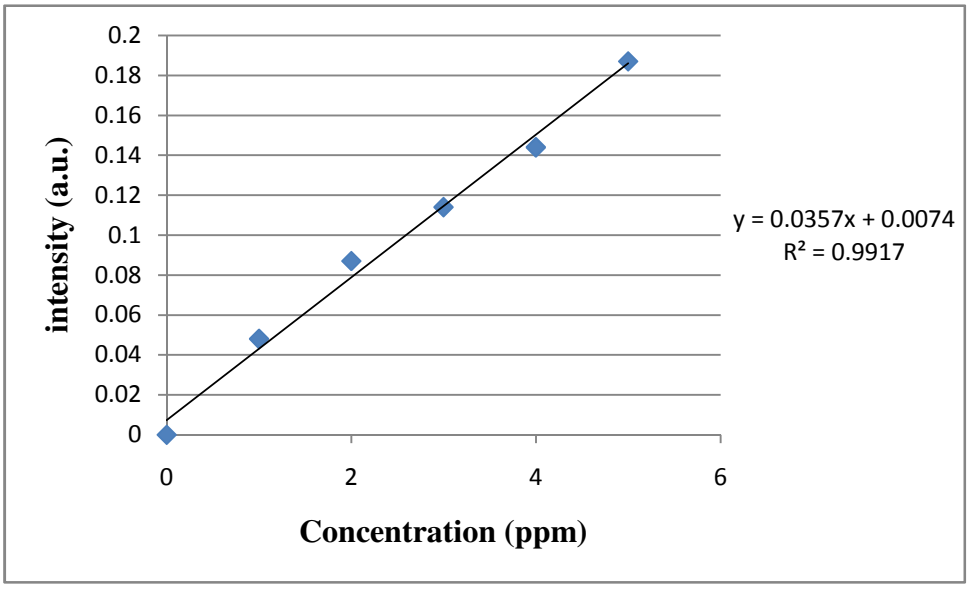

Figure 34d Calibration curve for Tin at 270.65 nm curve (2 µs delay, 3 µs gate width, 50 µm slit width, 300 avgs)

The detection limit was 0.9 ppm. A summary of analytical figures of merit is shown in table 32.

Table 32 Analytical figures of LIBS

Analytical Figures	**Te**	**As**	**Sn**
Limit of Detection (ppm)	1	1	0.9
Relative Standard Deviation (%)	0.4	0.9	0.6
Linear range (ppm)	1 to 5	1 to 5	1 to 5

Table 33 Comparison of LOD's of HG-LIBS with other techniques[102]

Method	**Te (ppb)**	**Sn (ppb)**	**As (ppb)**
Flame AA	30	150	150
Flame AA-HG	0.03	-	0.03
GFAA	0.1	0.1	0.05
ICP-MS	0.0008	0.005	0.006
HG-LIBS	750[103]	2700[104]	200[104]
HG-LIBS*	1000	900	1000
HG-ICP-AES*	1000	1000	-
HG-LIF*	0.008	0.07	-

The LODs obtained here for Te, Sn and As are higher than the current HG-LIF approach and to that reported previously and are comparable to the current HG-ICP-AES technique.

5.3.2.3. ENHANCEMENT EFFECT OF ETHANOL ON ARSENIC AND TIN SENSITIVITY

It has been reported that ethanol can enhance the sensitivity in HG measurements of As and Se.[105] The enhancement effect of ethanol on Arsenic and Tin sensitivity by HG-LIBS was studied by adding 0 mL, 1 mL, 2 mL, 3 mL, and 4 mL of ethanol to 5 ppm of Arsenic and Tin solutions. Instead of observing an increase in the signal as has been reported in the literature,[105] the HG-LIBS sensitivity was decreased for these elements. This result remains to be investigated further.

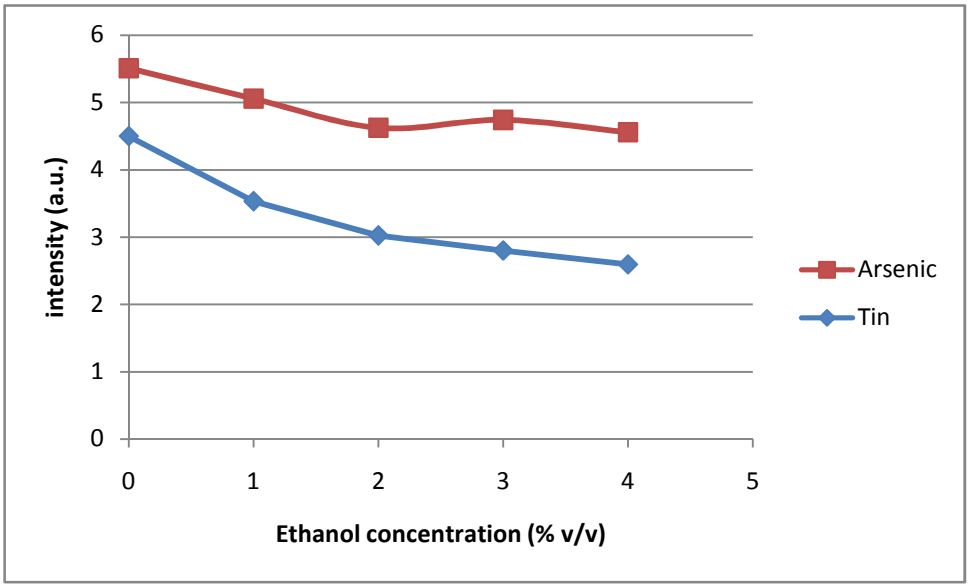

Figure 35 Enhancement effect of ethanol on Arsenic and Tin sensitivity

5.3.2.4. DETECTION OF DIFFERENT METALS IN A MIXTURE

A mixture containing Arsenic, Selenium and Antimony was subjected to LIBS. Emission lines of the different elements were observed at their respective emission wavelengths. This indicates that the HG-LIBS technique is suitable for multi-element analysis of samples containing hydride forming elements.

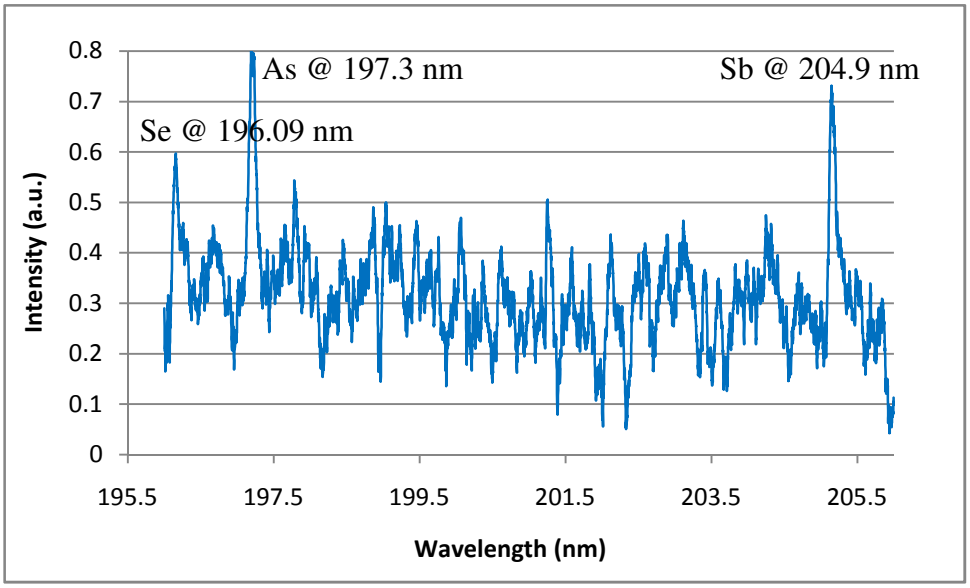

Figure 36 Detection of different metals in a mixture

5.3.2.5. HYDROGEN EMISSION SPECTRA

Due to the significant amounts of hydrogen introduced into the LIBS plasma when using HG, it was of interest to study the hydrogen spectra. Hydrogen atomic emission lines near 656 nm, 486 nm, and 434 nm were observed. By using these spectra, it is possible to study different plasma characteristics such as plasma temperatures and electron densities. The broadening of these emission lines depends on the electron density and their relative intensity depends on the plasma temperature. Future studies of the plasma characteristics will be useful for optimizing the detection of elements by the HG-LIBS approach.

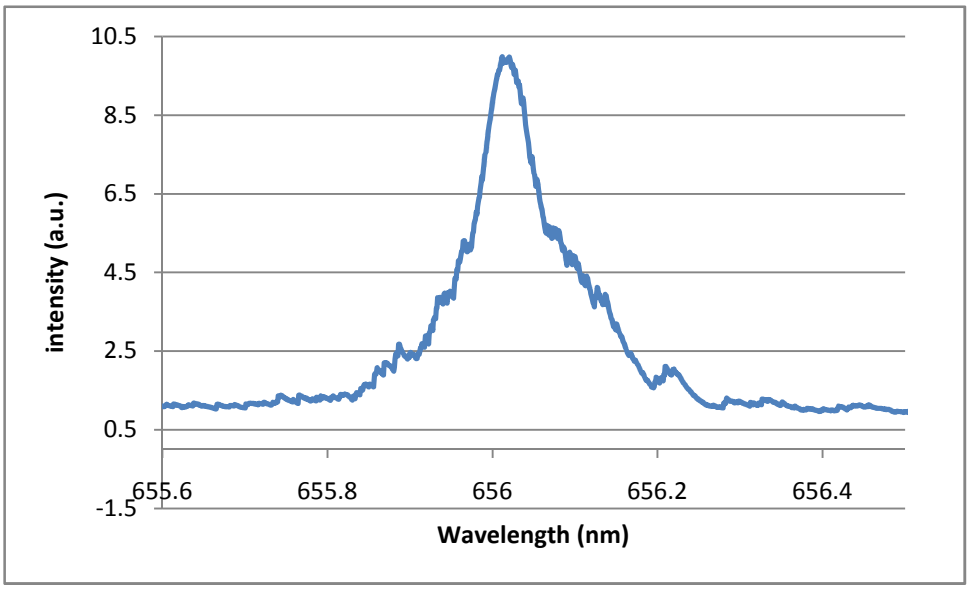

Figure 37a Hydrogen emission spectrum near 656 nm (2 µs delay, 200 ns gate width, 50 µm slit width and 30 avgs)

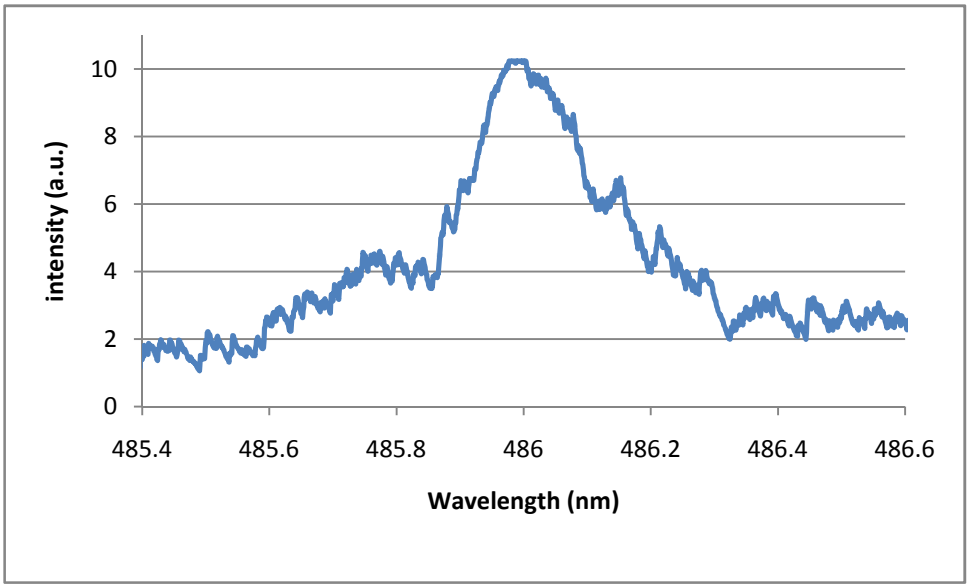

Figure 37b Hydrogen emission spectrum near 486 nm (2 µs delay, 200 ns gate width, 50 µm slit width and 30 avgs)

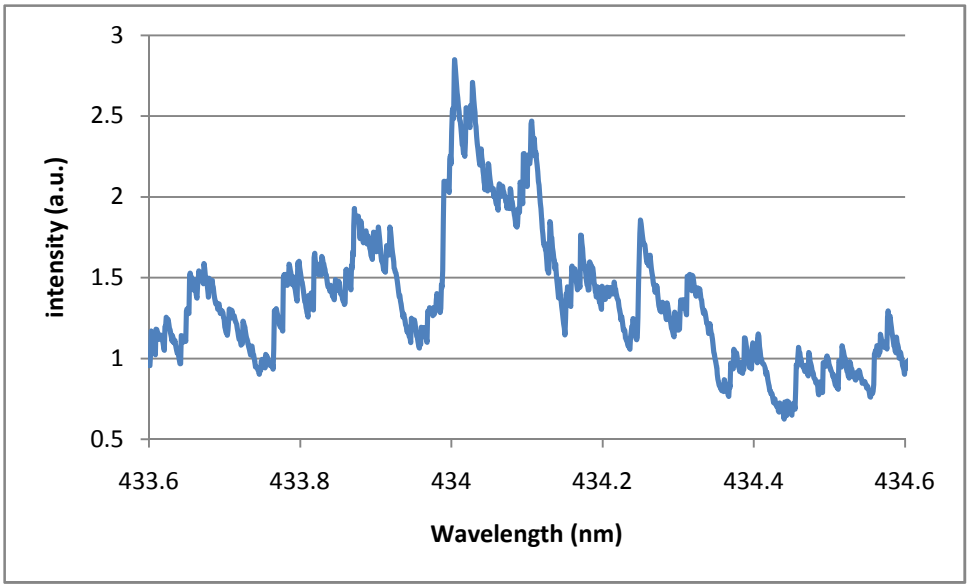

Figure 37c Hydrogen emission spectrum near 434 nm (2 µs delay, 200 ns gate width, 50 µm slit width and 30 avgs)

CHAPTER VI

CONCLUSIONS AND FUTURE WORK

The combination of hydride generation sample introduction with laser induced fluorescence detection has shown good linearity and very good detection limits for tellurium and tin. The obtained LODs by using HG-LIF are in the ppt range while they are in the ppb and ppm range using the corresponding ICP-AES and LIBS techniques. The HG-LIF results for Te are comparable to or better than most previously used techniques, including HG-ICP-MS. The obtained results for Sn-HG-LIF were good compared to ICP-AES and LIBS techniques, but are not better compared to all previously used techniques. In general, the LODs obtained for the ICP-AES techniques are in the ppb range and the combination of HG, did not improve the detection limits. This suggests that the HG system may not have been interfaced efficiently to the ICP system. While much less sensitive than HG-LIF, the HG-LIBS approach is better suited to multi-element analyses.

Future studies should include speciation measurements by selective reduction of Te (VI) to Te (IV), the minimization of Te memory effects, the enhancement of tin sensitivity, the combination of High Performance Liquid Chromatography (HPLC) approaches to the HG-LIF techniques, and the application of these approaches to the measurement of Te and Sn in environmental and biological samples. Further studies should also include the study of the LIBS plasma characteristics such as the temperature and electron density, improvement of the sensitivity, the speciation of As and the study of the enhancement effect of ethanol on other hydride forming elements.

Finally, it will be of interest to incorporate fiber optics into the LIBS approach to enable the use of smaller plasmas and possibly allow the measurement of smaller samples.

CHAPTER VII

REFERENCES

(1) Jain, C. K.; Ali, I. *Water Res*. **2000**, 34, 4304.

(2) Sjöström, S. *Spectrochim. Acta. Rev.* **1991**, 13, 407.

(3) Enger, J.; Marunkov, A.; Chekalin, N.; Axner, O. *J. Anal. At. Spectrom.* **1995***,* 10, 539.

(4) Bolshov, M. A. *Fresenius J. Anal. Chem.* **1996***,* 355, 549.

(5) Maessen, F. J. M. *Inductively Coupled Plasma Emission Spectroscopy*, Wiley, Newyork, 1987.

(6) Thompson, M.; Walsh, J. N. *Handbook of Inductively Coupled Plasma Spectroscopy,* Blackie, Glasgow, UK, 1983.

(7) Daskalova, N.; Velichkov, S.; Slavova, P. *Spectrochim. Acta, Part B.* **1996**, 51, 733.

(8) Ismail, M. A.; Imam, H.; Elhassan, A.; Youniss, W. T.; Harith, M. A. *J. Anal. At. Spectrom.* **2004**, 19, 489.

(9) Mohamed, W. T. Y. *Int. J. Pure. Appl. Phys.* **2006**, 2, 11.

(10) Radziemski, L. J. *Microchem. J.* **1994***, 50*, 218.

(11) Corsi, M.; Cristoforetti, G.; Palleschi. V.; Salvetti. A.; Tognoni. E. *Eur. Phys. J. D.* **2001**, 13, 373.

(12) Noll, R.; Bette, H.; Brysch, A.; Kraushaar, M.; Monch, I.; Peter, L.; Sturm, V. *Spectrochim. Acta, Part B.* **2001**, 56, 637.

(13) Salle, B.; Cremers, D. A.; Maurice. S.; Wiens, R. C. *Spectrochim. Acta, Part B.* **2005**, 60, 479.

(14) López-Moreno, C.; Palanco, S.; Laserna, J.; DeLucia, F.; Miziolek, A. W.; Walters, R. A.; Whitehouse, A. I. *J. Anal. At. Spectrom.* **2005***,* 21, 55.

(15) Samek, O.; Telle, H. H.; Beddows, D. C. S. *BMC Oral Health.* **2001**, 1, 1472.

(16) Windom, B. C.; Diwakar, P. K.; Hahn, D. W. *Spectrochim. Acta, Part B.* **2006***,* 61, 788.

(17) Carranza, J. E.; Hahn, D. W. *J. Anal. At. Spectrom.* **2002***,* 17, 1534.

(18) Arca, C.; Ciucci, A.; Palleschi, V.; Rastelli, S.; Tognoni, E. *Appl. Spectrosc.* **1997***,* 51, 1102.

(19) Berman, L. M.; Wolf, P. J. *Appl. Spectrosc.* **1998**, 52, 438.

(20) Cremers, D. A.; Radziemski, L. J.; Loree, T. R. *Appl. Spectrosc.* **1984***,* 38, 721.

(21) Knopp, R.; Scherbaum, F. J.; Kim, J. I. *Fresenius J. Anal. Chem.* **1996***,* 355, 16.

(22) Poulain, D. E.; Alexander, D. R. *Appl. Spectrosc.* **1995***,* 49, 569.

(23) Fichet, P.; Mauchien, P.; Wagner, J. F.; Moulin, C. *Anal. Chim. Acta.* **2001***,* 429, 269.

(24) Ho, W. F.; Ng, C. W.; Cheung, N. H. *Appl. Spectrosc.* **1997***,* 51, 87.

(25) Cheung, N. H.; Yeung, E. S. *Appl. Spectrosc.* **1993***,* 47, 882.

(26) Ng, C. W.; Ho, W. F.; Cheung, N. H. *Appl. Spectrosc.* **1997***,* 51, 976.

(27) Singh, J. P.; Zhang, H.; Yueh, F. y.; Carney, K. P. *Appl. Spectrosc.* **1996***,* 50, 764.

(28) Cheng, E. A. P.; Fraser, R. D.; Eden, J. G. *Appl. Spectrosc.* **1991***,* 45, 949.

(29) Radziemski, L. J.; Loree, T. R.; Cremers, D. A.; Hoffman, N. M. *Anal. Chem.* **1983**, 55, 1246.

(30) Rai, A. K.; Yueh, F.; Singh, J. P. *Appl. Opt.* **2003***,* 42, 2078.

(31) Body, D.; Chadwick, B. L. *Spectrochim. Acta, Part B.***2001***,* 56, 725.

(32) Shiue, M. Y.; Sun, Y. C.; Yang, M. H. *Analyst.* **2001***,*126, 1449.

(33) Krull, I.S. *Trace Metal Analysis and Speciation*. Elsevier, Amsterdam, **1991**, 226.

(34) Hashimoto, Y.; Sekine, Y.; *Bunseki*. **1990**, 2, 111.

(35) Taylor, A. *Biological Trace Element Research*. **1996**, 55, 231.

(36) Pacquette, H. L.; Elwood, S. A.; Ezer, M.; Simeonsson, J. B. *J. Anal. At. Spectrom.* **2001**, 16, 152.

(37) Casiot, C.; Barciela Alonso, M. C.; Boisson, J.; Donard, O. F. X.; Potin-Gautier, M. *Analyst.* **1998***,* 123, 2887.

(38) Maher, W.A. *Analyst.* **1983**, 108, 305.

(39) Pereiro, R.; Wu, M.; Broekaert, J. A. C.; Hieftje, G. M. *Spectrochim. Acta, Part B.* **1994,** 49, 59**.**

(40) Vinas, P.; Lopez-Garcia, I.; Merino-Merono, B.; Hernandez-Cordoba, M. *Appl. Organometal. Chem*. **2005**, 19, 930.

(41) Kobayashi, R.; Imaizumi, K. *Anal. Sci.* **1991**, 7, 841.

(42) Fodor, P.; Barnes, R. M. *Spectrochim. Acta, Part B.* **1983**, 38, 229.

(43) Zhang, L. S.; Combs, S. M. *J. Anal. At. Spectrom.* **1996**, 11, 1043.

(44) Klinkenberg, H.; Van-der-wal, S.; De-koster, C.; Bart, J. *J. Chromatogr. A.* **1998**, 794, 219.

(45) Kuo, C. Y.; Jiang, S. J. *J. Chromatogr. A*. **2008**, 1181, 60.

(46) Lindemann, T.; Prange, A.; Dannecker. W.; Neidhart, B.; *Fresenius. J. Anal. Chem*. **2000**, 368, 214.

(47) Rüdel, H. *Ecotoxicol. Environ. Saf.* **2003***,* 56, 180.

(48) Fent, K.; Hunn. *Environ. Sci. Technol*. **1991**, 25, 956.

(49) Bryan, G. W.; Burt, G. R.; Gibbs, P. E.; Pascoe, P. L. *J. Mar. Biol. Assoc.* ***1993****,* 73, 913.

(50) Mueller, M. D.; Renberg, L.; Rippen, G. *Chemosphere.* **1989**, 18, 2015.

(51) Perring, L.; Basic-Dvorzak, M. *Anal. Bioanal. Chem.* **2002***,* 374, 235.

(52) Department of Food Sanitation, the Ministry of Health and Welfare. *Study on tin-dissolving in canned juice*. Shokuhin Eisei Kenkyu. **1966**, 16, 871.

(53) D'Ulivo, A.; Bramanti, E.; Lampugnani, L.; Zamboni, R. *Spectrochim. Acta, Part B.* **2001**, 56, 1893.

(54) Ebdon, L.; Hill, S. J.; Jones, P. *Analyst.* **1985**, 110, 515.

(55) Grotti, M.; Rivaro, P.; Frache, R. *J. Anal. At. Spectrom*. **2001**, 16, 270.

(56) Nigge, W.; Marggraf, U.; Linsheid, M. *Fresenius J. Anal. Chem*. **1994**, 350, 533.

(57) Rivaro, P.; Zaratin, L.; Frache, R.; Mazzucotelli, A. *Analyst.* **1995**, 120, 1937.

(58) Chiron, S.; Roy, S.; Cottier, R.; Jeannot, R. *J. Chromatogr. A.* **2000**, 879, 137.

(59) Magi, E.; Ianni, C. *Anal. Chim. Acta.* **1998***,* 359, 237.

(60) Marshall, B. J. *Am. J. Gastroenterol.* **1991**, 86, 16.

(61) Gorbach, S. L. *Gastroenterology.* **1990**, 99, 863.

(62) Ross, J. F.; Broadwell, R.D.; Poston, M.R.; Lawhorn, G.T. *Toxicol. Appl. Pharmacol.* **1994**, 2, 124.

(63) Li, Z.; Guo, Y. *Talanta.* **2005***,* 65, 1318.

(64) Velitchkova, N.; Pentcheva, E. N.; Daskalova, N. *Spectrochim. Acta, Part B.* **2004**, 59, 871.

(65) Vanhoe, H.; Dams, R.; Versieck, J. *J. Anal. Atomic. Spectrom*. **1994**, 9, 23.

(66) Chen, S.; Zhang, Z.; Yu, H. *Anal. Bioanal. Chem.* **2002**, 374, 126.

(67) Feng, Y. L.; Chen, H. Y.; Chen, H. W.; Tian, L. C. *Fresenius J. Anal. Chem.* **1998**, 361, 155.

(68) Zhang, L. S.; Combs, S. M. *J. Anal. At. Spectrom.* **1996**, 11, 1043.

(69) Gerber, G. B.; Leonard, A. *Mutat. Res.* **1997**. 387. 141.

(70) Zhe-Min, N.; Bi, H. *J. Anal. At. Spectrom.* **1995**, 10, 747.

(71) Dagnall, R. M.; Kirkbright, G. F.; West, T. S.; Wood, R. *Analyst.* **1970**, 95, 425.

(72) Tseng, C. M.; Amouroux, D.; Brindle, I. D.; Donard, O. F. X. *J. Envi. Moni.* **2000**, 2, 603.

(73) Böyükbayram, A. E.; Volkan, M. *Spectrochim. Acta, Part B.* **2000**, 55, 1071.

(74) Guo, X. M.; Guo, X. M. *Anal. Chim. Acta.* **1998**, 373, 303.

(75) Mortlock, R. A.; Froelich, P. N. *Anal. Chim. Acta.* **1996**, 332, 277.

(76) Nakahara, T.; Wasa, T. *Microchem. J.* **1994**, 49, 202.

(77) Giblin, A. *Handbook of Geochemical Exploration.* **1994**, p291.

(78) Price, W. J.; Roos, J. T. H.; Clay, A. F. *Analyst.* **1970**, 95, 760.

(79) Johansson, M.; Hansson, R.; Snell, J.; Frech, W. *Analyst.* **1998**, 123, 1223.

(80) Armentrout, D. N. *Anal. Chem.* **1966**, 38, 1235.

(81) Ferreira, S. L. C.; Brito, C. F.; Dantas, A. F.; Araújo, N. M. L.; Costa, A. C. S. *Talanta.* **1999**, 48, 1173.

(82) Yunes, N.; Moyano, S.; Cerutti, S.; Gásquez, J. A.; Martinez, L. D. *Talanta.* **2003**,59, 943.

(83) Park, C. J.; Yim, S. A. *J. Anal. At. Spectrom.* **1999**, 14, 1061.

(84) Mester, Z.; Fodor. P. *Spectrochim. Acta, Part B*. **1997**, 52, 1763.

(85) Bohari, Y.; Astruc, A.; Astruc, M.; Cloud, J. *J. Anal. At. Spectrom*. **2001**, 16, 774.

(86) García, J. B.; Krachler, M.; Chen, B.; Shotyk, W. *Anal. Chim. Acta.* **2005**, 534, 255.

(87) Miravet, R.; López-Sánchez, J. F.; Rubio, R. *Anal. Chim. Acta*. **2004**, 511, 295.

(88) Montesinos. P. C,; Guardia. A,; Teutsch. C,; Cervera. M. L,; Guardia. M. *J. Anal. At. Spectrom*. **2004**, 19, 696.

(89) Raymann, P. M.; Abou-Shakra, R. F.; Ward, N. I. *J. Anal. At. Spectrom*. **1998**, 11, 61.

(90) Sturgeon, R. E.; Willie, S. N.; Sproule, G. I.; *Spectrochim. Acta, Part B*. **1989**, 44, 667.

(91) Vuchkova, L.; Arpadjan, S. *Talanta*. **1996**, 43, 479.

(92) Moreda-Pineira, J.; Cervera, L. M.; Guardia, M. *J. Anal. At. Spectrom*. **1997**, 12, 1377.

(93) Rabada, J. M.; Galba, J.; Vida, J. C.; Aznare, J. *J. Anal. At. Spectrom.* **1990**, 5, 45.

(94) Feng, Y. L.; Narasaki, H.; Chen, H. Y.; Tian, L. C. *Fresenius J. Anal. Chem.* **1997**, 357, 822.

(95) Corns, W. T.; Stockwell, P. B.; Ebdon, L.; Hill, S. J. *J. Anal. At. Spectrom.* **1993**, 8, 71.

(96) Fairbank, W. M.; Hansch, T. W.; Schawlow, A. L. *J. Opt. Soc. Am.* **1975**, 65, 199.

(97) She, C. Y.; Fairbank, W. M.; Billman, K. W. *Opt. Lett.* **1978**, 2, 30.

(98) Fassel, J. D.; Crouch, S. R. *Spectrochemical Analyst,* Englewood Cliffs, NJ, 1988.

(99) Dedina, J.; Tsalev, D. *Hydride Generation and Atomic Absorption Spectrometry,* Wiley, New York, 1995.

(100) Cremers, D.; Radziemski, L. *Hand Book of Laser Induced Breakdown Spectroscopy,* Wiley, NewYork, 2006.

(101) *Experimental Transition Probabilities for Spectral Lines of 70 Elements,* United States National Bureau of Standards, 1961.

(102) *Guide to Inorganic Analysis,* PerkinElmer Inc., 2004, 005139C, KG070420.

(103) May, J. L.; Alexander, J.; *Laser Induced Plasma, A versatile tool for chemical analysis,* Idaho national engineering and environmental laboratory.

(104) Fortes, F. J.; Cortes, M.; Cabalin, L. M.; Laserna, J. J. *Anal. Chem. Acta.* **2005**, 136, 554.

(105) Qiu, P.; Ai, C.; Lin, L.; Wu, J.; Ye, F. *Microchem. J.* **2007**, 87, 1.